Real-Time Global Localization of a Mobile Robot by Exploiting RFID Technology

Anastasios Tzitzis, *Student Member, IEEE,* Alexandros Filotheou, Aristidis Raptopoulos Chatzistefanou, Traianos Yioultsis, *Member, IEEE,* Antonis G. Dimitriou, *Senior Member, IEEE*

***Abstract*—This work addresses the problem of the global localization of a mobile robot by exploiting RFID technology. The robot is equipped with kinematic sensors capable of measuring the incremental distances covered by each wheel and an RFID reader which measures the phase of the signal that is backscattered by reference RFID tags situated inside the environment at known positions. The motion of the robot with respect to the tags enables the collection of measurements from multiple antenna-locations, in a synthetic-aperture sense. Localization of the mobile robot over time is accomplished by processing short segments of trajectory during each iteration. The odometry-data are exploited to estimate each segment of the vehicle's trajectory relative to an unknown initial position. The odometry-based estimation, the known positions of the reference tags, the unwrapped phase measurements and a phase-to-distance model represent the input to a data-fit problem, the solution of which reveals the unknown initial position and orientation of the trajectory segment in the absolute frame. Thanks to phase unwrapping, the data-fit problem features convexity-type properties and the solution is rapidly found by non-linear optimization techniques. The influence of different algorithmic features on the performance of the method is investigated in a simulative context. An experimental campaign that employs a prototype robotic agent equipped with two antennas reports a mean absolute localization error of less than 0.1m, while the execution time stays below the measurements' collection-time such that the real-time capability of the method is preserved.**

***Index Terms*—Radio Frequency Identification, RFID, Robot Tracking, Global Localization, synthetic aperture, Nonlinear Optimization, Phase Unwrapping, Robotics, Odometry.**

I. Introduction

In recent years, references to the term "smart environment", an environment in which sensors, machines and computers interact with everyday objects and people, have become increasingly common. At the same time autonomous robotic vehicles can extract all the necessary information about objects without human intervention, fully automating every process. In such an intelligent world, self-localization of any mobile robot is quite a significant feature, and inextricably linked to multiple tasks, such as autonomous navigation, localization of surrounding objects, mapping, etc.

A great variety of approaches has been developed to address the problem of localizing a robotic agent. Among others, dead reckoning [1] represents a simple solution, according to which odometry-data, gathered by proprioceptive sensors, such as wheel encoders and accelerometers, are used to determine the change of the robot's position and orientation relatively to previous ones. Nevertheless such techniques are characterized by their inability to address the global localization problem, i.e. when no information about the robot's initial pose is given. Instead, they recover the robot's location in a local reference frame that is not related to the actual environment. Furthermore, due to their low accuracy, proprioceptive sensors produce erroneous estimations. Most importantly, the measurement errors increase with time, leading eventually to diverging discrepancies between the actual and the estimated trajectory.

To avoid cumulative errors, as well as to be capable of determining the absolute location of the robot inside the environment, the employment of exteroceptive sensors represents an essential feature of any localization system, i.e. sensors that transduce information concerning the outside world. RGB(D) cameras, LIDARs, sonars, etc, are installed on board the robotic vehicle and obtain external measurements, which in most scenarios represent distances from reference landmarks [2] - [10]. A robot's ability to locate itself globally requires its awareness of the landmarks' positions, namely the environment's map. The problem where those locations are unknown and the robot has to estimate both them and its own pose is referred as Simultaneous Localization and Mapping, also known as SLAM [11].

Although exteroceptive sensors are in general characterized by low measurement error, their effectiveness depends strongly on a clear visual field and deteriorates when obstacles such as people walk in front of them, i.e. when their field of view is obstructed. Under such circumstances, the robot becomes unable to locate itself within the map. As a consequence, it fails to navigate in the environment. Such behavior was experienced in the Archaeological Museum of Thessaloniki where a robot designed to play treasure-games with younger visitors and classes of 20-25 students was installed. The robot is equipped with a 360° LIDAR for accurate localization. Though the system performs robustly under partly crowded conditions, when the children are present, the robot fails to update its pose, eventually failing to fulfill its navigation-missions.

This research has been co-financed by the European Union and Greek national funds through the Operational Program Competitiveness, Entrepreneurship and Innovation, under the call RESEARCH – CREATE – INNOVATE (project code:T2EDK-02000).

This research is part of the doctoral thesis of Anastasios Tzitzis, the implementation of which has been co-financed by Greece and the European Union (European Social Fund-ESF) through the Operational Programme Human Resources Development, Education and Lifelong Learning in the context of the Act "Enhancing Human Resources Research Potential by undertaking a Doctoral Research", Sub-action 2: IKY Scholarship Programme for PhD candidates in the Greek Universities

All authors are with the School of Electrical and Computer Engineering, Aristotle University of Thessaloniki, Greece, e-mail: antodimi@ece.auth.gr.

A. RFID-based Localization

Among exteroceptive technologies, RFID has attracted a lot of interest lately. Its low cost, high read-rate capabilities, and visually-contactless operability are among its main benefits over conventional optical technologies. An RFID-based robot localization scheme is typically realised by employing an RFID reader connected to one or multiple antennas on the robotic vehicle, while RFID tags are situated in the environment representing artificial landmarks, Fig. 1. In essence, the tags' coordinates define the absolute reference frame in which the robot is being localized [12].

The detection of a tag by the robot's reader implies that the latter is positioned withing the reading range of the reader's antenna. As a result, by utilizing the information of tag readability, a region of space can be determined in which the robot may be located. In such a framework, various methods have been presented in the literature. By employing a dense grid of RFID tags on the floor or ceiling, the locus of the robot's position can be reduced and the localization precision increased.

[13] deals with the global localization problem by exploiting only the binary information of a tag being detected or not. According to the identified tags, the region of space that the robot may be positioned is determined. This information is fused with odometry data through a Kalman-filter approach in order to perform a more precise estimation. [14] models the probability of a tag being detected by the reader depending on their distance. Robot position is released by estimating its speed and applying a weighted centroid localization algorithm. Similarly, [15] attempts to model the probability of a successful tag detection based on the reader's and the tag's locations. That information is fused with odometry readings through a particle filter approach so as to estimate the traversed path of the robot. [16] exploits RFID-based fingerprinting maps to identify positions that the robot may have revisited. A graph-based algorithm fuses odometry and RFID readings to estimate the robot's trajectory without requiring any information about the tags locations. In [17], the robot estimates its position in social scenarios where it is supposed to interact with people. A Support Vector Machine (SVM) learning classification technique based on the detected tags is proposed to determine the region of space the robot may be situated.

Two other types of information that may be utilized for localization are the received signal strength indication (RSSI) and the phase of the signal that is backscattered from a detected tag to the reader. Those quantities can be measured by any commercial RFID reader and from such measurements the distance between the tag and the reader's antenna can be extracted through theoretical models. RSSI is a variable inversely proportional to the antenna-to-tag distance through a path-loss model. However, it is quite sensitive to various factors such as the tag's orientation, the chip's model, the antenna's polarization, the material of the tagged surface, etc. Those are difficult to be predicted, leading in general, to unreliable models with poor accuracy.

In [18], RSSI measurements are inputted into a log-distance path loss model capable of estimating the tag-to-reader distances. The performance is enhanced by an iterative algorithm that corrects the model to account for a tag-reader angle-path loss factor and improve the accuracy. Reader location is finally recovered through trilateration. [19] employs a set of RFID tags on the floor and two antennas facing downwards. The proposed scheme requires an offline phase to receive RSSI measurements from multiple predefined locations. During the online phase, a prediction of the robot's position is made on the basis of odometry data while the estimated position is corrected by comparing the collected RSSI measurements with those received offline. [20] proposes a kalman filter implementation to mitigate the multipath effect on the RSSI measurements before they are inputted into the path-loss model. In [21], a finite impulse response (FIR) filter takes the place of the Kalman filter presuming robustness under industrial conditions.

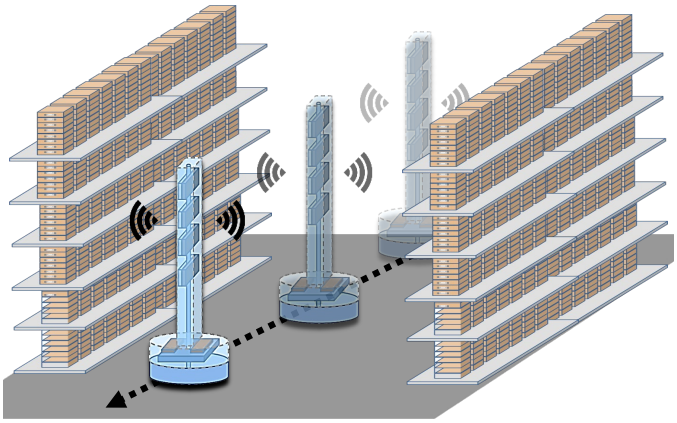

Fig. 1: An RFID-based robot localization scenario inside a warehouse environment. The robotic agent carries an RFID reader, while RFID tags are placed on the surrounding shelves.

In contrast to RSSI measurements, phase features a tolerance towards the above effects but suffers from a so-called cycle ambiguity. Phase has a periodic dependence on the antenna-tag distance and repeats for every half-wavelength change of it. In addition to the inherent 2π ambiguity, phase is also affected by the employed RFID equipment which introduces an unknown drift. As a result, the true value of distance cannot be directly inferred by a single phase measurement unless those ambiguities are treated properly.

[22] deals with the global localization problem, by fusing odometry readings and phase measurements from tags installed on the ceiling through a multi hypothesis kalman filtering. Phase measurements are used directly to reflect distance measurements on the condition that the unknown phase drifts have been filtered out during an offline calibration procedure. [23] utilizes a combination of both RSSI and phase measurements to avoid the preliminary calibration stage. An unscented Kalman filter fuses the RSSI with encoder data to provide among others an estimation of the unknown phase cycle. Once the latter is considered reliable enough, an extended kalman filter involves the phase measurements to further improve the pose estimation. Both [22] and [23] employ custom-made tags that are highly directive. In this

vein, the detection region is bounded near the antenna-tag Line-Of-Sight (LOS), thus mitigating the effects of multipath and providing more accurate phase and RSSI measurements.

In [24], kinematic readings are combined with the information of tag readability and measured phase differences through a particle filter algorithm. A classification strategy based on readability is also developed to reject improbable particles and increase accuracy. In order to define the readability space required for the classification algorithm, a tag is placed at various test points during a preparatory stage and it is recorded whether it is detected or not. Such manual procedure has to be repeated for different setups. [25] introduces the employment of the "TriLateration Tag", a special structure consisted of three closely-spaced tags, while the 2π ambiguity is dropped by using a phase difference of arrival (PDoA) approach. In [26], the problem's local and global observability is verified. A two-step kalman filter processes odometry readings to predict the robot's pose and phase differences of RFID signals to estimate the radial speed and update the predicted pose.

An alternative approach to deal with the phase ambiguity is to take advantage of the relative motion between the robot's antenna(s) and the stationary tags situated in the environment. In such manner, multiple measurements collected by several antenna locations are processed such that a synthetic aperture (SAR) is resembled. SAR-based methods estimate the robot's pose on the basis of sequences of phase measurements instead of a single one.

A SAR-based method is presented in [27], which exploits readings from kinematic sensors to construct a trajectory that is relative to an unknown initial point. By processing the phase measurements collected along the driven trajectory, the initial position is recovered in a maximum likelihood sense, while knowledge of the phase ambiguity is released by considering phase differences. The solution is sought by employing a population of particles each of which represents a hypothetical robot location. The performance of such search methods depend strongly on the number of test points since the more the investigated locations the greater the expected accuracy, at the expense of increased computational cost and execution time. In the same context, [28] simulates a conveyor belt scenario and the relative trajectory of the transponder is extracted thanks to knowledge of the belt's speed. The maximum likelihood problem is then solved by performing an exhaustive search over a grid of possible points along the search-space, introducing even higher computational complexity.

Besides the robot-localization problems, RFID technology has been widely used to solve a variety of similar problems such as the robot-navigation and SLAM. [29] addresses a navigation problem, where the robot has been assigned the mission of approaching a static tag. By comparing RSSI measurements collected from different orientations of the robot, the bearing of the target tag is discovered and a movement towards that direction is decided. In [30], the robot is able to recognise the motion of a tag through a RSSI-based dynamic model. Being integrated into a local path planner, such information achieves object tracking and obstacle avoidance. [31] faces a navigation problem according to which the robot is given a set of successive points that define its desired trajectory. It employs a RSSI-to-distance transformation to calculate the distances from all detected tags while the pose of the robot is represented as the solution of a particle swarm optimization problem.

[32] deals with the problem of estimating the robot's trajectory while simultaneously localizing a set of reference beacons positioned in the external environment (SLAM). A Rao-Blackwellized Particle Filtering algorithm integrates odometry data and phase measurements of RFID tags situated on the ceiling of the area. The RFID-based SLAM problem is also addressed in [33]. A multihypothesis extended Kalman filter is applied on the basis of measured phases and encoder readings to estimate the range and the bearing of each tag with respect to the robot. Furthermore, a phase-based navigation scheme is presented in [34], according to which the robot has to follow a moving tag. The relative angle between the robot and the tag is estimated by observing phase measurements collected from two robot-mounted antennas, while a particle filtering algorithm is implemented to keep track of the movement over time.

B. Contributions

This paper presents a novel method that addresses the problem of the global localization of a mobile robot, i.e. the problem of retrieving the robot's position and orientation in the global frame of reference, without any knowledge about the robot's initial state. The robot is realised as a differential-drive vehicle that moves by means of two independently-powered and -controlled wheels. The proposed solution suggests the robotic agent be equipped with kinematic sensors on its wheels to measure the incremental distances covered by each, while an RFID reader connected to two laterally mounted antennas facing towards opposite directions is installed as well on board the vehicle, Fig. 1. RFID tags positioned at known locations around the environment act as artificial landmarks and define the absolute coordinate system in which the robot is localized.

Tracking of the mobile robot over time is accomplished by processing short segments of trajectory each time. Odometry data collected by the wheel encoders are utilized to estimate the locations of each trajectory-segment relative to an unknown initial position and orientation. The relative motion between the robot and the tags allows for the collection of RFID measurements from multiple locations and, under such perspective, a synthetic aperture is resembled. The odometry-based relative trajectory of the robot-mounted antennas, the known positions of the surrounding RFID tags, the unwrapped phase measurements collected by them, and a phase-to-distance theoretical model represent the input to a data-fit problem, the solution of which reveals the unknown initial location and orientation of trajectory-segment in the absolute frame, accompanied by an estimation of the unknown phase drift. Thanks to phase unwrapping, the data-fit problem features convexity-type properties and the solution is rapidly found by non-linear optimization techniques. As a consequence, the real-time capability of the method is preserved. This approach has already been introduced in [35] - [37] under the name

"Phase ReLock" to localize a stationary tag by an RFID-augmented moving robot.

In contrast to other phase-based localization methods, the proposed scheme can be implemented using only commercial off-the-shelf (COTS) hardware, while it does not require any preparatory work regarding the calibration of the unknown phase drift. Instead, the phase offset is included as a parameter in the optimization problem and is estimated together with the robot's pose. This is feasible thanks to the fact that the proposed scheme exploits mobility to embody the synthetic aperture technique. Processing long series of measurements collected by multiple antenna locations makes the implementation of phase unwrapping feasible and the problem of the phase ambiguity resolvable. After all, treating long sequences of samples instead of one observation to estimate a single robot pose is expected to mitigate multipath and noise effects, thus allowing for a better performance.

Furthermore, contrarily to other SAR-based techniques, the presented method is independent of either a grid of hypothetical robot locations or a particle population. The robot's pose is retrieved by rapidly solving a non-linear optimization problem. Thanks to this property, the method can be easily implemented in real-time applications where the robot's position is updated frequently enough depending on the application requirements. All of these characteristics can be advantageous for real-world applications, demonstrating the method's broad potential for vehicle-localization uses.

The rest of the paper is organised as follows. Section II defines the system and measurement models. Section III presents the localization problem and illustrates the main ideas and the approach employed to solve the problem. The effectiveness of the proposed method is investigated through simulative tests in Section IV and in an experimental context in Section V. Finally, the conclusions are discussed in Section VI.

II. System Model

A. Robot Kinematics

Fig. 2 illustrates the kinematics of a differential-drive-like vehicle. Differential drive is a common driving system used by mobile robots. It comprises two driving wheels mounted on either side of the robot at a distance l_{RL}. The position situated halfway between the wheels is regarded as the robot's origin $\boldsymbol{A}_r$, while its heading θ_r is perceived with respect to the x-axis. The wheels may rotate independently; by altering the relative rate and direction of their rotation, the robot can follow different trajectories, follow either a straight path, or perform turns and maneuvers.

An encoder situated on the wheel is capable of measuring the distance travelled by the wheel within a given time interval. Let d_R^k and d_L^k denote the measured incremental distances that the right and left wheel have covered, respectively, within the interval between time instants k and $k+1$.

The position of the robot's origin $\boldsymbol{A}_r^k = [x_r^k, y_r^k, z_r^k]^T$ accompanied by its orientation θ_r^k serve as the robot's state at time instant k. Since a terrestrial robotic agent can move only in the x-y plane, the z-coordinate remains constant and is in fact equal to 0. According to the vehicle's drive kinematics, its temporal evolution is based on the previous state estimate such that:

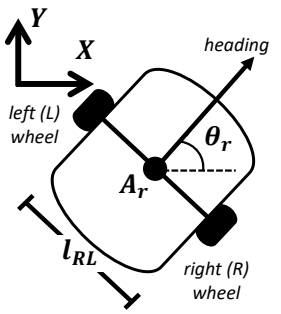

Fig. 2: Differential drive kinematics of a mobile vehicle

$$\theta_r^k = \theta_r^{k-1} + \frac{d_R^{k-1} - d_L^{k-1}}{l_{RL}} \tag{1}$$

$$\boldsymbol{A}_r^k = \boldsymbol{A}_r^{k-1} + \begin{bmatrix} \frac{d_R^{k-1} + d_L^{k-1}}{2} \cos\left(\theta_r^{k-1}\right) \\ \frac{d_R^{k-1} + d_L^{k-1}}{2} \sin\left(\theta_r^{k-1}\right) \\ 0 \end{bmatrix} \tag{2}$$

Consequently, the robot's pose at any time step k can be expressed with respect to its initial position $\boldsymbol{A}_r^1$ and direction θ_r^1:

$$\begin{aligned} \theta_r^k &= \theta_r^1 + \sum_{l=1}^{k-1} \frac{d_R^l - d_L^l}{l_{RL}} \\ &\triangleq f_{\theta_r}\left(\theta_r^1, \boldsymbol{d}^k\right) \end{aligned} \tag{3}$$

$$\begin{aligned} \boldsymbol{A}_r^k &= \boldsymbol{A}_r^1 + \begin{bmatrix} \sum_{l=1}^{k-1} \frac{d_R^l + d_L^l}{2} \cos\left(\theta_r^l\right) \\ \sum_{l=1}^{k-1} \frac{d_R^l + d_L^l}{2} \sin\left(\theta_r^l\right) \\ 0 \end{bmatrix} \\ &\triangleq \boldsymbol{A}_r^1 + f_{A_r}\left(\theta_r^1, \boldsymbol{d}^k\right) \end{aligned} \tag{4}$$

where vector $\boldsymbol{d}^k = [d_R^1, d_L^1, \cdots, d_R^{k-1}, d_L^{k-1}]$ includes all encoder measurements collected up to time step $k-1$. Equations (3) - (4) can produce a trajectory that is relative to an initial pose $(\boldsymbol{A}_r^1, \theta_r^1)$. Given different initial poses, different trajectories are created, all of which however, have same shape, as indicated in Fig 3.

In addition to wheel encoders, an RFID reader connected to multiple antennas is mounted on board the mobile vehicle. The location of the center of the j^{th} out of N_A antennas at time instant k is denoted $\boldsymbol{A}_{a,j}^k = [x_{a,j}^k, y_{a,j}^k, z_{a,j}^k]^T$ and is related to the vehicle's origin $\boldsymbol{A}_r^k$ according to:

$$\begin{aligned} \boldsymbol{A}_{a,j}^k &= \boldsymbol{A}_r^k + \begin{bmatrix} \cos\left(\theta_r^k\right) & -\sin\left(\theta_r^k\right) & 0 \\ \sin\left(\theta_r^k\right) & \cos\left(\theta_r^k\right) & 0 \\ 0 & 0 & 1 \end{bmatrix} \begin{bmatrix} \Delta x_{a,j} \\ \Delta y_{a,j} \\ \Delta z_{a,j} \end{bmatrix} = \\ &\triangleq \boldsymbol{A}_r^k + R\left(\theta_r^k\right) \Delta A_{a,j} \end{aligned} \tag{5}$$

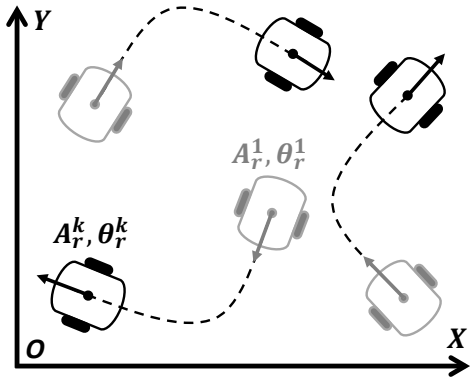

Fig. 3: Depending on the initial pose of the robot, equations (3) and (4) produce a different trajectory in the absolute frame of reference. Each of them, though, may be regarded as a rotated and translated copy of the other

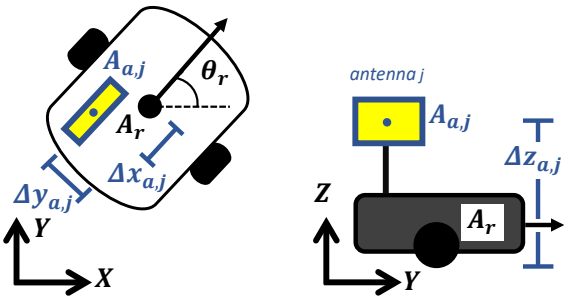

Fig. 4: Geometry of the RFID equipment installed on board the mobile robot.

with $\Delta A_{a,j}$ being a three-element vector that includes the distances between the installed antenna's and robot's centers along the $x-$, $y-$ and $z-$ axis, as illustrated in Fig. 4. Those values are known a-priori. Furthermore, the antenna position is dependent on the robot's orientation θ_r^k through the operation of rotation represented by $R(\theta_r^k)$.

Eventually, by utilizing the robot's kinematic model (3) - (4), the temporal evolution of the antenna can be expressed with respect to the initial robot pose $(\boldsymbol{A}_r^1, \theta_r^1)$ such that:

$$\begin{aligned}\boldsymbol{A}_{a,j}^k &= \boldsymbol{A}_r^1 + f_{A_r}\left(\theta_r^1, \boldsymbol{d}^k\right) + R\left(f_{\theta_r}\left(\theta_r^1, \boldsymbol{d}^k\right)\right)\Delta A_{a,j} \\ &\triangleq \boldsymbol{A}_r^1 + F_{a,j}\left(\theta_r^1, \boldsymbol{d}^k\right). \end{aligned} \tag{6}$$

B. Phase Measurements

The relative motion of the robot with respect to the stationary tags, which are positioned around the environment, enables tag-readings from multiple antenna locations, resembling thus, the synthetic-aperture approach. Let the position of the i^{th} out of N_T tags be $\boldsymbol{A}_{t,i} = [x_{t,i}, y_{t,i}, z_{t,i}]^T$. Each tag-reading corresponds to the recording of the phase of the tag's backscattered signal. Without loss of generality, the tag readings and the kinematic data collected by the wheel encoders are assumed to be collected at same instants, such that any phase measurement is accompanied by the corresponding odometry-based information of the antenna's position. Fig. 5 (b) depicts

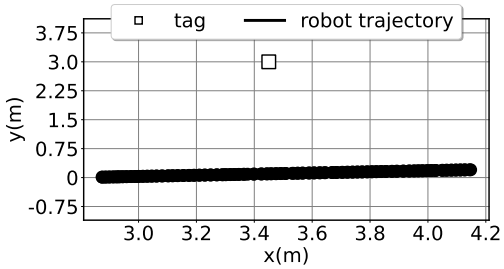

(a) The trajectory of the robot along which phase measurements are collected.

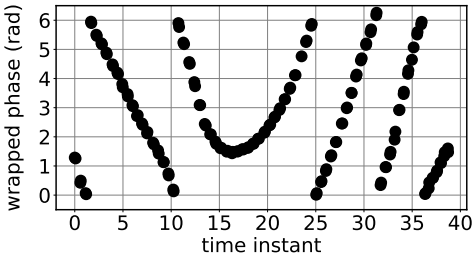

(b) Wrapped phase measurements with respect to the time instant of collection.

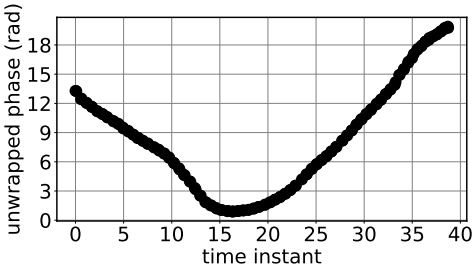

(c) Unwrapped phase samples with respect to the time instant of collection.

Fig. 5: Phase Unwrapping eliminates the 2π jumps and produces a continuous curve with support in $(-\infty, +\infty)$.

the phase curve measured along the synthetic aperture of Fig. 5 (a).

Let ϕ_{ij}^k denote the phase of the i^{th} tag measured by the j^{th} reader's antenna at time instant k. Phase can be modelled on the basis of the distance between those two:

$$\overline{\phi}_{ij}^k = \left(\frac{4\pi}{\lambda}\left\|\boldsymbol{A}_{a,j}^k - \boldsymbol{A}_{t,i}\right\| + c_{ij}\right) \mod 2\pi \tag{7}$$

where $\|\boldsymbol{A}_{a,j}^k - \boldsymbol{A}_{t,i}\|$ is given by:

$$\begin{aligned}&\|\boldsymbol{A}_{a,j}^k - \boldsymbol{A}_{t,i}\| = \\ &= \sqrt{(x_{a,j}^k - x_{t,i})^2 + (y_{a,j}^k - y_{t,i})^2 + (z_{a,j}^k - z_{t,i})^2}\end{aligned} \tag{8}$$

In (7), the former term of the summation corresponds to phase rotation over the signal's round-trip, i.e. forth and backward propagation, and λ stands for the wavelength of the carrier frequency. The term c_{ij}, is an extra shift induced by the setup's electronics, such as antennas' cables, tags' and reader's circuits, etc. Nevertheless, this drift is constant across all phase measurements corresponding to the same antenna-tag pair.

The resulting output of (7) is a remainder to 2π, to indicate that phase takes values only in intervals of 2π, as shown in Fig 5 (b). Measured phase is characterized by a periodicity. It repeats for every $\lambda/2$ change of the antenna-to-tag distance. As a consequence, it is unable to reflect the actual distance. Instead, all values that differ from one another by increments of half wavelengths would deliver the same phase. The introduced ambiguity can be tackled by performing phase unwrapping. This process aims to eliminate the phase jumps and drops that occur every 2π, by appropriately adding multiples of 2π to each measured sample. Fig. 5 (c) presents the reconstructed phase curve, which is free of discontinuities and unwrapped to $(-\infty, +\infty)$. The unwrapped phase can now be modeled by:

$$\overline{\phi}_{ij}^{k} = \frac{4\pi}{\lambda} \left\| \boldsymbol{A}_{a,j}^{k} - \boldsymbol{A}_{t,i} \right\| + c_{ij} \tag{9}$$

By integrating (6) in the above theoretical model, phase can be associated to the robot's initial pose such that:

$$\overline{\phi}_{ij}^{k} = \frac{4\pi}{\lambda} \left\| \boldsymbol{A}_{r}^{1} + F_{a,j}\left(\theta_{r}^{1}, \boldsymbol{d}^{k}\right) - \boldsymbol{A}_{t,i} \right\| + c_{ij} \tag{10}$$

III. Solution Approach

A. Overview

Localization of the robot is performed by processing data collected within a time window. The wheel-encoders' measurements are fed in (3) - (4) and the trajectory-segment travelled by the robot during that interval is calculated with respect to an **unknown** initial position and orientation. Those values are estimated by exploiting the phase measurements gathered by the tags situated in the surrounding environment. In such framework, the absolute location of the robot is recovered. By continuously processing successive segments of trajectory in such manner, tracking of the mobile robot over time is accomplished. Fig. 6 provides an intuition of the described procedure.

Success of the algorithm is based on exploiting the following properties. Odometry is not expected to suffer from large errors during small traveled segments. So the algorithm trusts odometry data as far as it concerns the distances between successive closely-spaced samples over a small displacement. Then the algorithm attempts to rotate and move each new segment throughout the map, in order to better fit its actual position (only the starting point and its orientation) based on phase-measurements collected by RFID tags. In that manner, it does not allow odometry errors to drift the current estimated position of the robot away from its actual position. Furthermore, a wealth of measured phases along each antenna-tag pair is used to calculate only four unknown parameters; the unknown drift of the measurements and the initial position and orientation of the current segment, trusting that all subsequent locations are well predicted by odometry. This overdetermined system is expected to mitigate multipath and noise effects in the richness of measurements trying to calculate only four unknowns.

Let the whole trajectory be split into non-overlapped segments of equal length; each segment consists of K time instants. For now on and without loss of generality, the notation

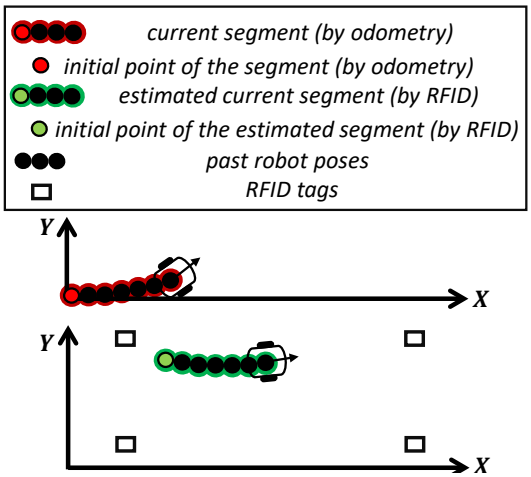

(a) Estimation of the first trajectory-segment. By utilizing the odometry readings the trajectory of the robot is reproduced (red). Not being able to initially know the origin of the absolute frame of the environment, the robot produces a trajectory by considering its initial position as the origin of the frame and its initial motion direction as the x axis. By utilizing the phase measurements of the tags, the trajectory is re-located (green) in the absolute reference frame which corresponds to the coordinate system of the RFID tags.

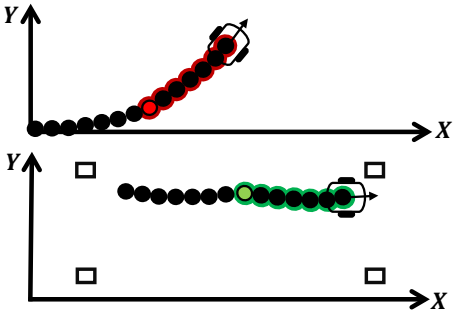

(b) Estimation of the second trajectory-segment.

Fig. 6: Initial steps of the proposed tracking method (part 1/2).

(n, k) will be fostered to represent the k^{th}, $k \in [1, K]$ time instant of the current trajectory segment n. In the remaining paper n refers to the latest/current segment that the algorithm is trying to place at the best position in the map. Contextually, the notation of all variables introduced throughout the paper are modified such that $\boldsymbol{A}_{r}^{n,k}, \theta_{r}^{n,k}, \boldsymbol{A}_{a,j}^{n,k}, \phi_{ij}^{n,k}$ and $\overline{\phi}_{ij}^{n,k}$ represent the position and orientation of the robot, the location of the j^{th} antenna, the measured and theoretical phase sample at the k^{th} time instant of the current trajectory segment n, respectively. Vector $\boldsymbol{d}^{n,k}$ includes the odometry data collected from the 1^{st} up to the $(k-1)^{th}$ instant of the current segment.

B. Segment Estimation

As discussed earlier, the estimation of the current trajectory segment refers to the estimation of its initial location and its initial orientation. All subsequent positions of the segment are taken by odometry data. This process takes place at the end of the corresponding trajectory segment, namely at time

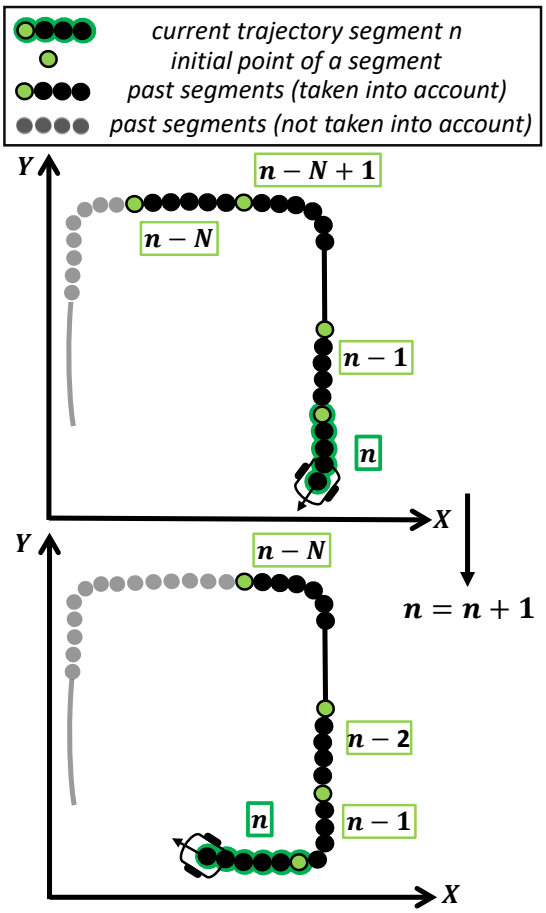

Fig. 7: The estimation of current trajectory segment n is accomplished by taking into account the previous segments $[n-N, n-1]$.

instant (n, K). As a result, the segment's length K essentially represents the estimation step since the robot's pose is updated every K time instants.

The unknown initial values are determined on the basis of data collected upon the current segment, together with data received during the N previous travelled segments, as illustrated in Fig. 7. Those segments correspond to a trajectory of NK instants length. Assuming that any previous segment m with $m < n$ has been already estimated, the poses of the robot and the locations of each antenna at time instants (m,k), $k \in [1,K]$, $m \in [n-N, n-1]$ are known. Those quantities are denoted as $\boldsymbol{A}_{r,est}^{m,k}, \theta_{r,est}^{m,k}$ and $\boldsymbol{A}_{a,j,est}^{m,k}$, respectively.

By inputting the collected phase measurements $\phi_{ij}^{n,k}$ and kinematic data $\boldsymbol{d}^{n,k}$ into the phase-distance model (10), a system of equations is crafted. Considering the pair of the j^{th} antenna and i^{th} tag, such system is obtained by:

$$
S_{ij}^{n}\begin{cases}
\begin{cases}
\phi_{ij}^{n-N,1} = \dfrac{4\pi}{\lambda}\left\|\boldsymbol{A}_{a,j,est}^{n-N,1} - \boldsymbol{A}_{t,i}\right\| + c_{ij} \\
\phi_{ij}^{n-N,2} = \dfrac{4\pi}{\lambda}\left\|\boldsymbol{A}_{a,j,est}^{n-N,2} - \boldsymbol{A}_{t,i}\right\| + c_{ij} \\
\vdots \\
\phi_{ij}^{n-N,K} = \dfrac{4\pi}{\lambda}\left\|\boldsymbol{A}_{a,j,est}^{n-N,K} - \boldsymbol{A}_{t,i}\right\| + c_{ij}
\end{cases} \\
\vdots \\
\begin{cases}
\phi_{ij}^{n-1,1} = \dfrac{4\pi}{\lambda}\left\|\boldsymbol{A}_{a,j,est}^{n-1,1} - \boldsymbol{A}_{t,i}\right\| + c_{ij} \\
\phi_{ij}^{n-1,2} = \dfrac{4\pi}{\lambda}\left\|\boldsymbol{A}_{a,j,est}^{n-1,2} - \boldsymbol{A}_{t,i}\right\| + c_{ij} \\
\vdots \\
\phi_{ij}^{n-1,K} = \dfrac{4\pi}{\lambda}\left\|\boldsymbol{A}_{a,j,est}^{n-1,K} - \boldsymbol{A}_{t,i}\right\| + c_{ij}
\end{cases} \\
\begin{cases}
\phi_{ij}^{n,1} = \dfrac{4\pi}{\lambda}\left\|\boldsymbol{A}_{r}^{n,1} + F_{a,j}(\theta_{r}^{n,1}, \boldsymbol{d}^{n,1}) - \boldsymbol{A}_{t,i}\right\| + c_{ij} \\
\phi_{ij}^{n,2} = \dfrac{4\pi}{\lambda}\left\|\boldsymbol{A}_{r}^{n,1} + F_{a,j}(\theta_{r}^{n,1}, \boldsymbol{d}^{n,2}) - \boldsymbol{A}_{t,i}\right\| + c_{ij} \\
\vdots \\
\phi_{ij}^{n,K} = \dfrac{4\pi}{\lambda}\left\|\boldsymbol{A}_{r}^{n,1} + F_{a,j}(\theta_{r}^{n,1}, \boldsymbol{d}^{n,K}) - \boldsymbol{A}_{t,i}\right\| + c_{ij}
\end{cases}
\end{cases}
$$

The last K equations refer to the current segment n and contain four unknown parameters: the x- and y- coordinates of the robot's initial position in $\boldsymbol{A}_r^{n,1}$, the robot's initial orientation $\theta_r^{n,1}$ and the offset of the phase curve c_{ij}. The first K equations correspond to the $(n-N)^{th}$ trajectory-segment which has already been estimated in a previous step, so the antenna locations $\boldsymbol{A}_{a,j,est}^{n-N,k}$, $k \in [1,K]$ are available. The unknown quantity of those equations is one, namely the phase offset c_{ij} which is common for all phase measurements of the link between the j^{th} antenna and the i^{th} tag. Eventually, by considering all of the N estimated segments, the crafted system consists of $(N+1)K$ equations and four unknown parameters.

The number N affects the system's degrees of freedom (df), i.e. a measure that quantifies the amount of information available to estimate a parameter. In general, having more degrees of freedom can make it easier to estimate the unknown parameters accurately. By having more equations, the effects of noise or multipath in individual measurements can be averaged out, resulting in a more accurate solution. In this case, since the phase offset c_{ij} is the parameter that appears in all $(N+1)K$ equations, the number N directly affects the confidence and accuracy of its estimation. Having such a precise estimation for one of the system's unknowns facilitates the accurate estimation of the remaining parameters as well, namely initial position $\boldsymbol{A}_r^{n,1}$ and orientation $\theta_r^{n,1}$, even though they are included only in the last K equations.

Additionally, being common for all phase measurements of the specific antenna-tag pair, the unknown phase drift c_{ij} essentially associates the current segment n with the N previous ones. Through the estimation of the phase offset, the algorithm estimates the initial pose of the current segment by taking into account the estimated locations of the previous segments $\boldsymbol{A}_{r,est}^{n-N,k}$ as well. As a result, the algorithm is

expected to locate each current segment at least at the vicinity of its previous one, thus producing an overall trajectory with no significant discontinuities between consecutive segments, as it will be demonstrated in section V.

Assuming there are $N_T N_A$ available antenna-tag links, each of which corresponds to a similar set of $(N+1)K$ equations, an augmented system can be crafted to account for all antennas and tags. Such system $S^n = \{S^n_{11}, \cdots, S^n_{N_T N_A}\}$ has $N_T N_A (N+1)K$ equations and $3 + N_T N_A$ unknown parameters; the x- and y- coordinates of robot's initial location $\boldsymbol{A}_r^{n,1}$ at the n^{th} segment, its initial orientation $\theta_r^{n,1}$ and the $N_T N_A$ phase curve offsets of the involved antenna-to-tag pairs. The above quantities are represented by vector $\boldsymbol{p} = (\boldsymbol{A}_r^{n,1}, \theta_r^{n,1}, c_{11}, \cdots, c_{N_T N_A})$.

System S^n resembles a data-fit problem where the measured phase samples should best match the theoretical ones given by (10). Since the system is overdetermined, the least squares method is employed to determine the solution, and the ideal parameters are sought such that they produce the minimum sum of squared differences between the observed and theoretical phase values:

$$\boldsymbol{p}_{est} = \arg\min_{\boldsymbol{p}} P(\boldsymbol{p}) \tag{11}$$

The matching function $P(\cdot)$ follows:

$$P(\boldsymbol{p}) = \sum_{m=n-N}^{n} \sum_{k=1}^{K} \left[\sum_{i=1}^{N_T} \sum_{j=1}^{N_A} \left(\Delta\phi_{ij}^{m,k}(\boldsymbol{p}) \right)^2 \right] \tag{12}$$

where $\Delta\phi_{ij}^{m,k}$ represents the difference between the measured and theoretical phase at time instant (m,k) that corresponds to the pair of the j^{th} antenna and i^{th} tag:

$$\Delta\phi_{ij}^{m,k} = \begin{cases} \phi_{ij}^{m,k} - \dfrac{4\pi}{\lambda} \left\| \boldsymbol{A}_{a,j,est}^{m,k} - \boldsymbol{A}_{t,i} \right\| - c_{ij}, \\ \qquad\qquad if\ n - N \leq m < n \\ \phi_{ij}^{m,k} - \dfrac{4\pi}{\lambda} \left\| \boldsymbol{A}_r^{m,1} + F_{a,j}\left(\theta_r^{m,1}, \boldsymbol{d}^{m,k}\right) - \boldsymbol{A}_{t,i} \right\| + \\ \qquad\qquad -c_{ij}, \quad if\ m = n \end{cases} \tag{13}$$

Eventually the remaining robot poses of the current segment are computed by (3) - (4):

$$\begin{aligned} \theta_{r,est}^{n,k} &= f_{\theta_r}\left(\theta_{r,est}^{n,1}, \boldsymbol{d}^{n,k}\right),\ k \in [2,K] \\ \boldsymbol{A}_{r,est}^{n,k} &= \boldsymbol{A}_{r,est}^{n,1} + f_{A_r}\left(\theta_{r,est}^{n,1}, \boldsymbol{d}^{n,k}\right),\ k \in [2,K] \end{aligned} \tag{14}$$

while those of each antenna are computed according to (5):

$$\boldsymbol{A}_{a,j,est}^{n,k} = \boldsymbol{A}_{r,est}^{n,k} + R\left(\theta_{r,est}^{n,k}\right) \Delta A_{a,j},\ k \in [1,K],\ j \in [1,N_A] \tag{15}$$

The described procedure is summarized in Algorithm 1.

Algorithm 1: Estimation of current segment n

- **Data:** i) the phase measurements and the odometry data of current trajectory segment and ii) the phase measurements and the estimated locations of the antennas during the previous N segments
- **Result:** i) the poses of the robot and ii) the positions of the antennas during the current trajectory segment
- **Step 1:** Create the relative robot route with respect to its unknown initial position and orientation by (3) - (4)
- **Step 2:** Compute the route of each antenna with respect to the robot's unknown initial position and orientation by (6)
- **Step 3:** Solve data-fit problem (11) by non linear optimization and obtain the optimum initial position and orientation of the robot
- **Step 4:** Compute the remaining poses of the trajectory by (14)
- **Step 5:** Compute the locations of each employed antenna by (15)

C. Non Linear Optimization

Being nonlinear to its unknown parameters, objective function P is unable to be resolved using a closed form. Instead, nonlinear optimization that makes use of iterative techniques allows for minimization over the parameter space [40] - [42]. The method starts with an initial guess of the unknown parameters and iteratively modifies them so as the function repeatedly decreases and the fit improves. When certain convergence requirements are satisfied and a minimum is attained, the process comes to an end. However, getting the best values of the unknown parameter-vector entails identifying the global minimum of the objective function instead of a local one. Therefore, the latter should demonstrate a single minimum in the domain such that non-linear optimization is feasible. However, the objective function P is not convex in the entire parameter-domain and does not experience a single global minimum.

Let the case where the robot is equipped with two directional patch antennas, facing opposite directions to the left and to the right with respect to the forward direction of movement of the robot, as is the actual deployed case. A single series of tags is placed to the left of the direction of movement. Due to the antennas' directional pattern, the tags are only detected by the left antenna. To this point, the algorithm has no knowledge that the tags should be to the left of the robot's trajectory, given that they have been interrogated by the left antenna. The algorithm, so far, treats each antenna as being omni-directional along the x-y plane and therefore the data identified by the left antenna, could equiprobably exist to the right of the direction of motion. The corresponding resultant cost function P is shown in Fig. 8 and the two possible robot trajectories in Fig. 9. Indeed, two minima are demonstrated and depending on the initial (x,y) coordinates in the optimization problem, the algorithm will converge to one of them, failing to guarantee that the proper minimum has been reached. Similarly, according to the tag-setup and the problem's geometry, other cases of symmetry can be reported along the x-y plane.

Another symmetry, which leads to two local minima, emerges along the parameter-direction of the orientation $\theta_r^{n,1}$.

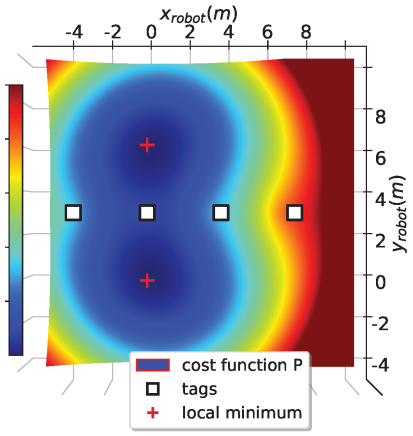

Fig. 8: Representation of matching function P along the parameter plane $x_r^{n,1} - y_r^{n,1}$. Higher amplitudes of P are represented by hotter colors. Two minima are exhibited, which are symmetrical with respect to the sequence of the tags. Depending on the initial value of the optimization algorithm, a different minimum will be attained.

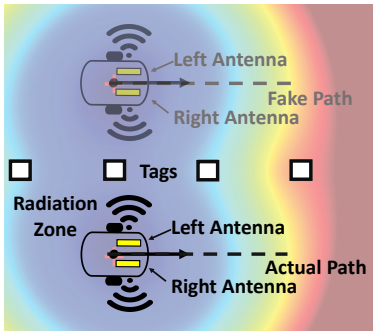

Fig. 9: Geometrical representation of the robot's two possible locations according to the cost function's minima is also shown. The "wrong" minimum will be discarded by considering the radiation pattern of the antennas with respect to the subset of measured tags.

This effect is shown in Fig. 10. In contrast to the symmetry along the x-y plane which arises from the identical measurements of the two possible trajectories, the orientation-ambiguity arises from the fact that $\theta_r^{n,1}$ is within cosines and sines in P, according to (4) - (6), always resulting in two local minima within $[0°, 360°)$ Again, depending on the starting value of the optimization algorithm, a different minimum will be attained. Fig. 11 shows the two possible robot orientations according to the minima of P in Fig. 10.

D. Initialization of the algorithm - Global Localization

Wrapping up, there are two sources of ambiguity: *i*) erroneous estimation of local minimum along the x-y plane and *ii*) erroneous estimation of the orientation of the robot. Those affect mainly the estimation of the first trajectory segment of the robot, since initially the robot can be placed anywhere inside the environment and no information about its starting location and heading is available, i.e. the problem of global localization. As a result, no assumption about the initial input of the optimization algorithm can be made.

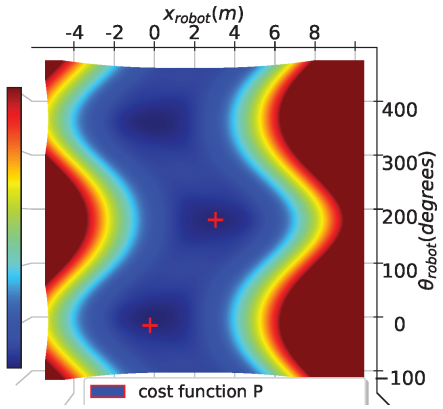

Fig. 10: Representation of matching function P along the parameter plane $x_r^{n,1} - \theta_r^{n,1}$. P exhibits two minima within [0,360°] which correspond to opposite robot's orientations. Depending on the initial value of the optimization algorithm, a different minimum will be attained.

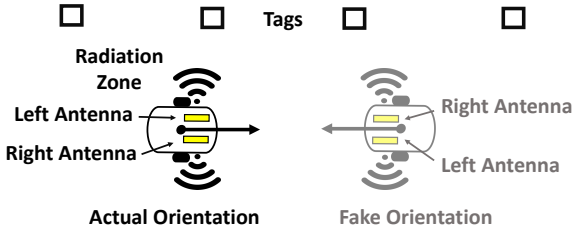

Fig. 11: Geometrical representation of the robot's two possible orientations according to the cost function's minima. By considering the radiation pattern of the antennas with respect to the subset of measured tags, the ambiguity is resolved and the "wrong" minimum can be discarded.

These ambiguities can be resolved by solving the optimization problem multiple times for different initial inputs. Let M points along the parameter-space of x-y and two directions for each point in $[0°, 360°)$ differing by $180°$. The optimization problem is executed independently for each of the $2M$ initial values, leading to $2M$ possible solutions (initial poses of the first segment). Among them, the best solution can be identified by considering the antennas' radiation pattern with respect to the measured subset of tags per antenna.

The antennas employed in most RFID applications are directional patch antennas, which mainly radiate in half-space; typical front-to-back ratio is greater than 15dB. As a result, depending on the robot's pose and the location they are installed on, they illuminate a certain area of the search-space and a group of tags. Let $D_{ij,exp}^{n,k}(p_{est}^{(l)})$ and $D_{ij,meas}^{n,k}$ denote the expected and the measured detection-state of the i^{th} tag, respectively, where $p_{est}^{(l)}$ with $l = 1, 2, \ldots, 2M$ represents the possible solutions of the optimization problem, initiated for M initial positions and two initial opposite directions for each position. $D_{ij,meas}^{n,k}$ takes a value of 1 if the i^{th} tag is actually detected by the j^{th} antenna at time instant (n, k) and $D_{ij,exp}^{n,k}(p_{est}^{(l)})$ takes a value of 1 in case the i^{th} tag is expected to fall within the reading range of the j^{th} antenna at time instant (n, k) if the robot's pose were determined by $p_{est}^{(l)}$. Otherwise, each value is set to zero. Each hypothesis $p_{est}^{(l)}$

representing the robot's pose is quantified by:

$$G\left(p_{est}^{(l)}\right)=\sum_{k=1}^{K}\sum_{i=1}^{N_T}\sum_{j=1}^{N_A}D_{ij,meas}^{n,k}D_{ij,exp}^{n,k}\left(p_{est}^{(l)}\right),$$
$$l=1,2,\ldots,2M \quad (16)$$

which is essentially proportional to the number of tags that are both actually and theoretically detected. Eventually, the value that corresponds to the maximum value of (16) is selected as the best solution:

$$p_{est}=\arg\max_{p_{est}^{(l)}}\{G\left(p_{est}^{(1)}\right),\cdots,G\left(p_{est}^{(l)}\right),\cdots,G\left(p_{est}^{(2M)}\right)\} \quad (17)$$

To account for the aforementioned uncertainties and perform global localization of the robot, during the calculation of the initial segment of the robot's trajectory, the procedure of Algorithm 2 is proposed.

Algorithm 2: Estimation of the initial segment

Data: i) the phase measurements and the odometry data collected upon the first segment

Result: i) the initial position and orientation of the robot and ii) the positions of the antennas during the first trajectory segment

Step 1: Wait until the robot has moved for an initial distance, e.g 50cm, based on data collected from the motion controller.

Step 2: Compute the route of each antenna with respect to the robot's unknown initial position and orientation by (6)

Step 3: Create the relative robot route with respect to its unknown initial position and orientation by (3) - (4)

Step 4: Cluster the measured tags.

Step 15: Create a search space comparable to a reader's read-region centered around the cluster with the largest tags' population, e.g. 10m×10m.

Step 6: Choose M uniformly spaced positions within the search space; e.g. every 1m.

Step 7: For each position, choose two opposite directions, randomly selected; e.g. 30° and 210°.

Step 8: Utilize each of the $2M$ hypothetical values as the initial input of the optimization algorithm and solve data-fit problem (11) $2M$ times

Step 9: Quantify the probability of each obtained solution by (16)

Step 10: Identify the best solution according to (17) which represents the estimated initial pose of the robot

Step 11: Compute the remaining poses of the trajectory by (14)

Step 12: Compute the locations of each employed antenna by (15)

This process needs to be executed only once to locate the first segment of the robot's trajectory. The estimated orientation and location of the first segment is inputted to the optimization algorithm as the initial parameter values of the next segment and so on. Provided that fake minima have been discarded by considering the radiation pattern of the antennas, the cost function is convex with respect to all variables of the problem. Such characteristic results, are shown in Fig 12 and Fig. 13, which illustrate the smooth surface of P along the parameter-planes of $x_r^{n,1}-c_{11}$ and $x_r^{n,1}-y_r^{n,1}$, respectively.

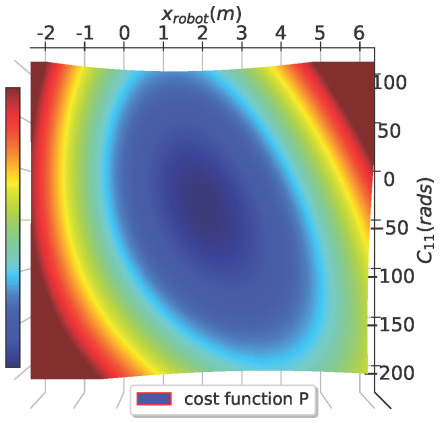

Fig. 12: Representation of matching function P along the parameter plane defined by the x- initial coordinate and the phase offset of a specific antenna-tag link $x_r^{n,1}-c_{11}$. The function's convex-type property is indicated by the smooth change in coloring.

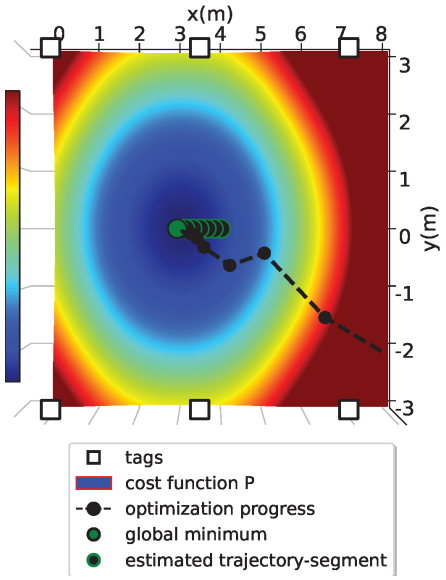

Fig. 13: Representation of matching function P along the parameter plane $x_r^{n,1}-y_r^{n,1}$. The function's convex-type property is indicated by the smooth change in coloring. The plot is enhanced by the progress of the optimization algorithm too, which iteratively converges to the minimum. Black circles correspond to the algorithm's estimation of the parameters $x_r^{n,1}$ and $y_r^{n,1}$ at each iteration, while the green circle refers to the optimum values.

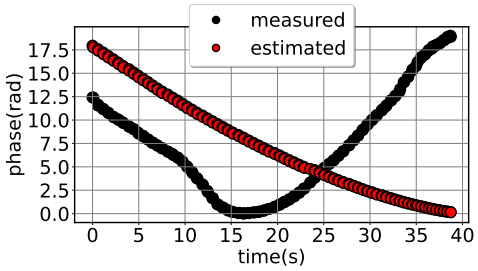

(a) Iteration 4: The estimated values represent a bad fit since the produced phase curves exhibit a significant discrepancy with the measurements.

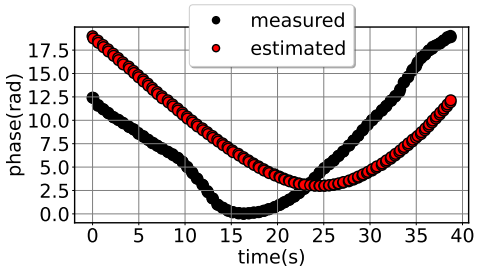

(b) Iteration 8: The estimated values are refined and deliver an improved matching, since they are closer to the optimal values. The difference between the theoretical phase curve and the measured one is significantly smaller than past iterations, but still far from optimum.

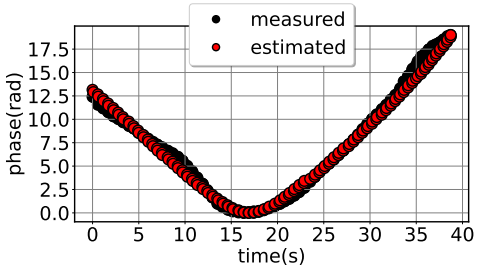

(c) Finally, the minimum of the cost function has been attained and the optimal parameter values (green circle in Fig. 13) deliver the best possible fit.

Fig. 14: Contrast between the measured unwrapped phase curves collected during the current trajectory-segment and the theoretical phase curves when the parameter values $\boldsymbol{p}$ that were estimated at different algorithm's iterations are inputted in equation (10).

E. Best-fit Solution

Fig. 13 shows the method's progress of converging to the function's desired minimum along the parameter directions of $x_r^{n,1}$ and $y_r^{n,1}$. The optimization algorithm starts with an initial selection of the unknown parameters and iteratively adjusts them (black circles) until it finally attains the minimum of the function, which corresponds to the best values (green circle). Likewise, Fig. 14 contrasts the estimated curve created for the parameters determined at various iterations of the algorithm with the phase curve measured by the antenna. Initially, there is a significant discrepancy between the measured and estimated data due to a poor choice of the starting values. However, via the repeated process, the closer the estimation is to the minimum, the more the created curve matches the measured one. The minimum is finally reached, and the best fit is achieved.

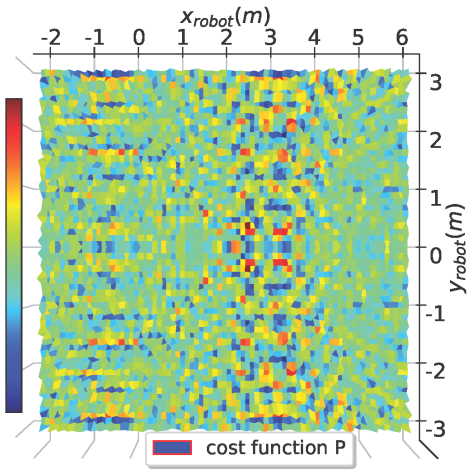

Fig. 15: Representation of matching function P along the parameter plane $x_r^{n,1} - y_r^{n,1}$, when no phase unwrapping is performed and the phase model (7) is employed. In contrast to Fig. 13, P suffers from multiple local minima and maxima making the application of non-linear optimization infeasible.

F. Necessity of Phase Unwrapping

Fig. 15 shows an illustration of matching function P along the parameter plane of the segment's x- and y- initial coordinates $x_r^{n,1} - y_r^{n,1}$ when no phase unwrapping is performed and the phase model (7) is applied. Notice that the dimensions of the space-domain are equal to the cost-function, shown in Fig.13, where phase-unwrapping was deployed. Due to the modulo operator in (7) and the exploitation of phase samples that are wrapped in 2π intervals, the cost function P suffers from multiple local minima and maxima. This effect would be destructive for any deployed algorithm, resulting in the convergence to one of the local minima, instead of the sought one, depending on the selected initial values of the parameters. As a consequence, alternative techniques should be fostered to solve the problem, such as a computationally expensive search over a grid of possible values. Phase-unwrapping enables the real-time capability of the proposed method, i.e. the time required to estimate the robot's pose is shorter than the time between two successive estimations.

G. Correction of the estimated trajectory

In general, SAR-based methods strongly depend on the amount of the processed data, particularly the phase measurements. Initially, the robot has not traversed a long path and the reader has collected a poor set of phase samples. Any localization method applied on such inadequate data would struggle to make an accurate estimation of any segment's initial pose. In this vein, the first segments are expected to be estimated with poor accuracy. This would mislead the upcoming estimations and deteriorate the quality of the robot's tracking.

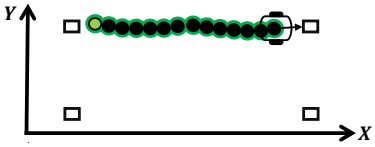

(a) After the estimation of the second trajectory segment (see Fig. 6), the whole estimated path is treated as a single segment and its initial position and orientation is re-estimated.

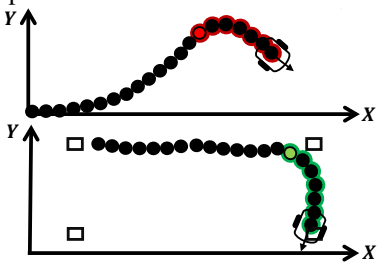

(b) Estimation of the third trajectory-segment.

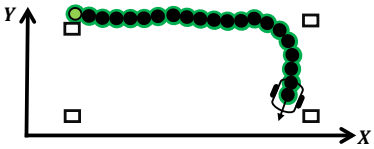

(c) After the estimation of the third segment, the whole estimated path is treated as a single segment and its initial position and orientation is re-estimated.

Fig. 16: Initial steps of the proposed tracking method (part 2/2).

To tackle this issue, after the estimation of a new segment n, the algorithm treats the estimated trajectory that corresponds to the previous segments $[n-N, n]$ as one common segment and aims to re-estimate the initial pose of the "super-segment" $(\boldsymbol{A}_r^{n-N,1}, \theta_r^{n-N,1})$. The idea is to move and rotate the entire "super-segment", composed of the latest N segments in space, so that the total error of the cost function is minimized. To accomplish that and avoid suffering from odometry-errors, only the position and orientation of the first sample of the 1^{st} out of N segments is considered as unknown. All subsequent positions are moved with respect to the first sample as calculated in the previous parts of the algorithm, where each segment was treated separately; the relative orientation of the 2^{nd} segment remains as calculated previously and so on. Fig. 16 demonstrates this process.

Such repetition is allowed thanks to the low computational cost of the algorithm. A non-linear optimization algorithm can converge to the problem's minimum rapidly estimating the initial pose of any segment in split seconds. As a result, this step introduces negligible complexity and the execution time required for the robot's localization hardly increases.

IV. Parameter Analysis

An excessive simulative analysis was carried out to investigate the impact of different algorithmic features on the performance of the localization. Fig. 17 shows the setup of the simulations: a differential drive robot moves in a "O"-shaped trajectory (grey color) inside a $5m \times 5m$ space while

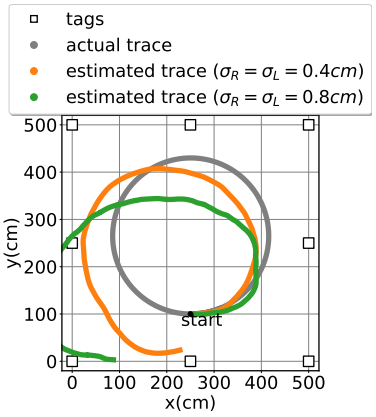

Fig. 17: Simulated actual and estimated trajectories based only on noisy odometry data. The initial position of the trajectory is known. Odometry-localization results in large errors.

eight tags are positioned in the surrounding environment. The robot traverses a path of a total length of $10\,\mathrm{m}$ completing one whole circle.

The simulated robot is equipped with an RFID reader and two laterally mounted antennas to collect phase measurements from the surrounding tags. The antennas are facing opposite directions illuminating different half-spaces. The reading zone of each of them corresponds to a width of 100° and only the tags that fall into it are successfully activated. Therefore, depending on the robot's position, measurements from different tags are available each time. In addition to the RFID equipment, kinematic sensors are placed on both wheels to obtain the distance travelled by each of them. Assuming that one phase and odometry reading is available approximately every $0.01\,\mathrm{m}$ of robot displacement, a set of about 1000 samples is collected.

A. Data Noise

To develop a realistic simulation model that accounts for data inaccuracies, both kinematic and RFID readings represent noisy measurements. As far the odometry data are concerned, those correspond to the erroneous measurement of each wheel's incremental distance $d_{R,n}$ and $d_{L,n}$ given by

$$\begin{aligned} d_{R,n} &= d_R + n_R \\ d_{L,n} &= d_L + n_L \end{aligned} \tag{18}$$

Quantities n_R and n_L are zero-mean Gaussian variables with standard deviation equal to σ_R and σ_L, respectively and d_R and d_L are the actual distances that essentially generate the circular trajectory of Fig. 17. By adjusting σ_R and σ_L, it is possible to experience different levels of sensor noise.

Regarding the phase measurement model of the RFID reader, it is designed to account for the multipath contribution as well. In all wireless systems, the received signal is a combination of signals following different paths. The latter correspond to the Line-of-Sight path and those generated through scattering and reflection in the propagation environment, referred as multipath. As a consequence, the reader is not able to extract the phase of the direct ray only, which is the

required information for precise localization, but it obtains the phase of the sum of all received rays, i.e. direct and reflected. According to the study in [43], the ratio of the direct field's strength to the mean of the multipath contribution is in the range of $4dBs$ to $12dBs$. This ratio determines to what extent the phase of the LOS ray is influenced.

Taking the above into consideration, the phase model employed through the numerical investigation is:

$$\phi = \phi_{LOS} + \phi_{mult} + \phi_{noise} \tag{19}$$

with ϕ_{LOS} representing the direct path obtained by (10), ϕ_{mult} modeling all reflected rays as one multipath contribution and ϕ_{noise} being of Gaussian nature with a standard deviation of $\sigma_\phi = 0.1$ rad. The multipath component ϕ_{mult} is given by

$$\phi_{mult} = \tan^{-1}\left(\frac{\rho \sin\delta\phi}{1+\rho\cos\delta\phi}\right) \tag{20}$$

where ρ determines the ratio of the direct ray's strength compared to the multipath ray; a value of zero refers to multipath absence, while a value of 1 represents equivalent strength between the multipath and the direct ray's contribution. The term $\delta\phi$ accounts for the difference between the phase of those rays and is modelled as a random variable uniform distributed in $[0, 2\pi]$.

The factors examined during the simulative analysis are the noise of the wheel encoder quantified by σ_R and σ_L in (18), the multipath conditions, quantified by the multipath-to-LOS ratio ρ introduced in (19), the number of employed antennas, the length of each segment K, which basically represents the estimation step and the number of previous segments N (i.e. the length of the previously traveled path) taken into account for the estimation of any current segment. Each simulation-test was repeated 1000 times in a Monte Carlo sense and the average results are presented and discussed.

B. Localization based on Odometry only

Initially, the robot localization is evaluated on the basis of odometry-only data, suffering from Gaussian encoder-noise, sized by σ_R and σ_L. The pose of the robot is estimated every $0.1\,\mathrm{m}$ of spatial displacement. Since the total traversed path is $10\,\mathrm{m}$ long, 100 estimations have been made.

Fig 17 demonstrates an example of trajectories estimated by using only noisy odometry data, assuming that the true initial point of the robot is given. Under such assumption, the estimated paths start from the same point, but the longer the robot has travelled the greater the error.

Fig. 18 quantifies that disagreement, by showing the localization error with respect to the travelled distance of the robot and different values of σ_R and σ_L. Since the start-point is known, the error is initially zero, but as time passes, the sensor measurement-error piles up leading to large localization errors. As expected, the localization error increases with the sensor noise. Even for small values (e.g. $\sigma_R = \sigma_L = 0.2cm$), the robot ends up being localized with a mean error greater than half meter, while worst accuracy is obtained for the higher tested value ($\sigma_R = \sigma_L = 1cm$) delivering localizing error greater than $2.5\,\mathrm{m}$.

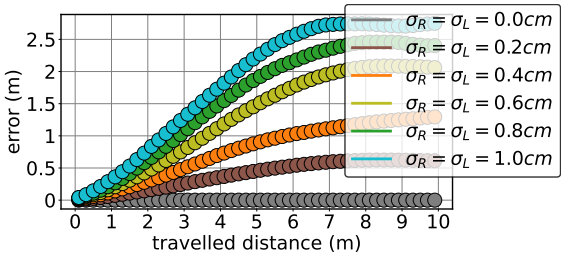

Fig. 18: Simulated localization error with respect to its travelled path when only odometry data are processed. Different levels of encoder noise are tested and presented.

C. Localization based on Odometry + RFID

The phase produced by (19) is exploited to correct the odometry errors. The multipath ratio is set to $\rho = 0.3$ and the standard deviation of phase $\sigma_\phi = 0.1$. As described in Section III-A, the tracking of the mobile robot is accomplished by processing successive trajectory segments of K instants. In this analysis, the whole trajectory is divided to segments of $0.1\,\mathrm{m}$. Since a new phase measurement and an encoder reading is assumed to be collected every $0.01\,\mathrm{m}$ of robot displacement, each trajectory segment contains 10 encoder and tag readings. Furthermore, the number of previous travelled segments taken into account are $N = 10$, a value that corresponds to $1\,\mathrm{m}$ of previously travelled path.

The global localization problem is addressed and no knowledge of the robot's initial position is available. Fig. 19 shows an example of estimated trajectories by employing 1 or 2 antennas. Exploiting data only from a single antenna has led to poor performance with the estimated trajectory having great dissimilarities compared to the actual one. On the contrary, the actual and the estimated path coincide when two antennas are used.

Fig. 20 and Fig. 21 compare the proposed method's performance for the cases of 1 and 2 deployed antennas, respectively. Both figures present the localization error with respect to the travelled distance of the robot and the noise of the odometry data. At first, the robot has traversed a short path and has collected only a few measurements. Since any SAR-based method depends on the number of collected data, such inadequate collection leads to poor performance and high localization error. Indeed, the first estimations are quite erroneous but quickly the error monotonically decreases as the robot travels longer path and more measurements are processed. After the first approximately $0.5\,\mathrm{m}$ of travelled distance, the error is stabilized and the method maintains its accuracy from then on.

However, the antenna population plays a key role. In the case of a single employed antenna (Fig. 20), the achieved error after the first steps ranges around $0.3\,\mathrm{m}$ depending on the level of sensor-noise. Contrarily, when two antennas are used, the error drops to zero (about $0.02\,\mathrm{m}$). This is quite an important observation, indicating that the proposed method operates better when measurements from tags placed at both sides of the robot are processed. As a consequence, the deployment of two antennas, each of which illuminates a different side of

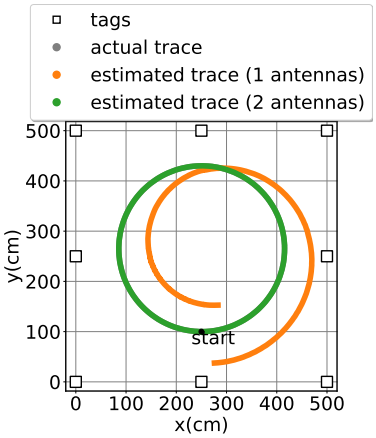

Fig. 19: Simulated actual and estimated trajectories when odometry and RFID data by a single or 2 antennas are combined. The initial position of the trajectory is unknown and the global localization problem is treated.

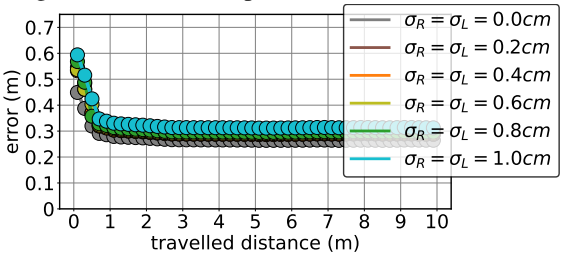

Fig. 20: Simulated localization error with respect to its travelled path when odometry data and RFID measurements by a single antenna are fused. Different levels of encoder noise are tested and presented.

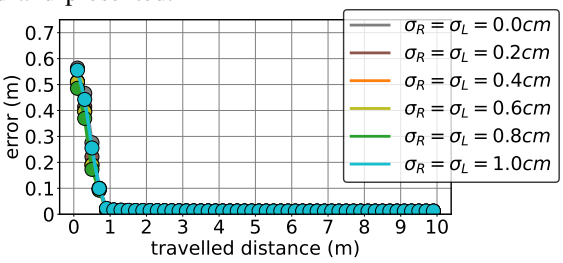

Fig. 21: Simulated localization error with respect to its travelled path when odometry data and RFID measurements by two antennas are fused. Different levels of encoder noise are tested and presented.

the search-space, represents a basic prerequisite for the proper operability of the method.

D. Performance vs Multipath Contribution

The contribution of multipath is evaluated, by testing different values of ratio ρ in (19). The results presented refer to a population of two deployed antennas. The standard deviation of the phase noise is set to $\sigma_\phi = 0.1$ and the standard deviation of the encoders' noise is $\sigma_R = \sigma_L = 1cm$. Each trajectory segment is $0.1\,\mathrm{m}$ long, while a previously travelled path of $1\,\mathrm{m}$ is taken into account by the algorithm.

Fig. 22 indicates the performance of the method is quite similar to the previous analysis. Initially, the estimations are

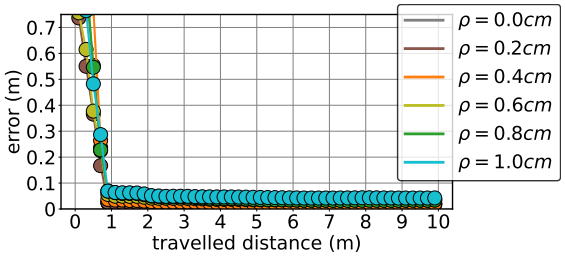

Fig. 22: Simulated localization error with respect to its travelled path when odometry data and RFID measurements by two antennas are fused. The RFID measurements suffer from multipath. Different values of multipath contribution are tested and presented.

poor leading to large errors, but after some steps, the error is stabilized around a certain value. Even for the worst case scenario of $\rho = 1$, i.e. equal contribution between multipath and direct link, the robot is being localized with a steady-state error around $0.05\,\mathrm{m}$. For smaller values of ratio the accuracy is slightly improved.

The equivalent accuracy reported for all values of ρ indicates that the method is robust to multipath. A single estimation is made on the basis of long travelled paths (in this case $1\,\mathrm{m}$ long), which lead to a wealth of phase samples. Processing such rich collections of data is expected to contribute to a significant mitigation of the multipath effect.

E. Performance vs Trajectory Segment Length, K

In this section, the performance of the method is investigated with respect to the length of each trajectory segment K. In general, the longer the segment, the more measurement-error induced by the wheel encoders is accumulated. As a direct result, an erroneous relative trajectory is produced by the odometry data and the estimation of the initial position of such an inaccurate trajectory will be poor as well. On the contrary, although short segments are expected to be only slightly affected by odometry errors, the poor collection of phase measurements along such segments would be inadequate to solve the optimization problem and provide with an accurate pose estimation.

Fig. 23 shows the achieved localization error for different values of sensor noise and segment length. Particularly, it demonstrates the steady-state error after the first executions of the algorithm. The standard deviation of the phase noise is set $\sigma_\phi = 0.1$, the multipath ratio $\rho = 0.3$ and two antennas are deployed. The length of the previously travelled path taken into account by the algorithm is set again to $1\,\mathrm{m}$.

When too short segments ($0.05\,\mathrm{m}$) are processed each time, the phase observations are not enough to estimate accurately the robot's pose. Especially at the beginning of the tracking process, a quite erroneous estimation can mislead the algorithm and force it to keep localizing the robot with great imprecision. This effect is indicated in Fig. 23, where a steady-state error of around $0.35\,\mathrm{m}$ is reported for all tested encoder noises. By slightly increasing the segment length, the performance is improved. No odometry error has been piled

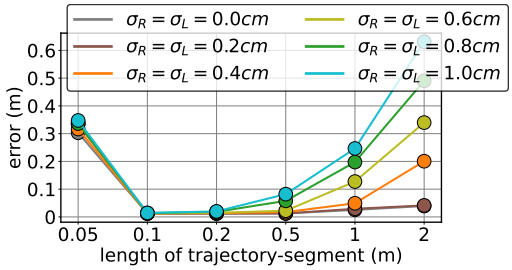

Fig. 23: Simulated localization error at steady with respect to the length of each trajectory segment when odometry data and RFID measurements by two antennas are combined. Different values of encoder noise are tested and presented.

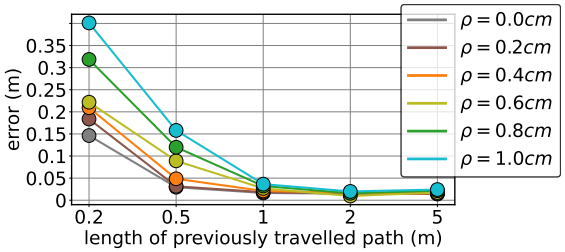

Fig. 24: Simulated localization error at steady state with respect to the length of the previously travelled path that is taken into account by the estimation-algorithm. Odometry data and RFID measurements by two antennas are combined. Different values of multipath contribution are tested and presented.

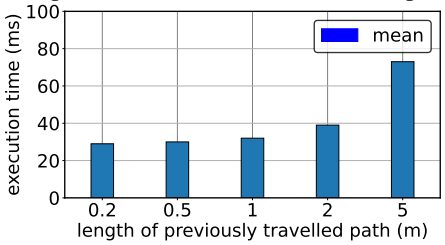

Fig. 25: Simulated execution time required for a single estimation of the robot's pose with respect to the length of the previously travelled path that is taken into account by the estimation-algorithm. Odometry data and RFID measurements by two antennas are exploited.

up in segments of ($0.1\,\mathrm{m}$ and $0.2\,\mathrm{m}$) length and the accuracy is hardly affected by the level of sensor-noise, delivering equivalent accuracy for all tested noise levels. Therefore, the impact of the sensor inaccuracies is negligible when short trajectory segments are utilized.

On the contrary, long segments are sensitive to the sensor noise and suffer from higher measurement-errors. For instance, when segments of $0.1\,\mathrm{m}$ are processed, a mean localization error of $0.08\,\mathrm{m}$ is achieved in the case of $\sigma_R = \sigma_L = 0.2cm$ and an error of $0.26\,\mathrm{m}$ in the case of $\sigma_R = \sigma_L = 1cm$. These values increase to $0.22\,\mathrm{m}$ and $0.65\,\mathrm{m}$, respectively when segments that are $2\,\mathrm{m}$ long are treated.

Fig. 23 indicates that a trade-off is introduced regarding the choice of the segment length. On one hand, the influence of the measurement noise increases with the increase of the segment length. Hence, the robot should be localized on the basis of short paths, such that the effect of the encoder noise on the method's performance is canceled out. On the other hand, long paths lead to richer collections of RFID measurements and the data-fit problem is better solved.

F. Performance vs Length of Previously Travelled Path considered, N

This analysis explores the method's effectiveness with respect to the length of the previously travelled trajectory taken into account for the estimation of a new trajectory segment. Being SAR-based, the proposed method depends on a wealth of collected readings to produce accurate estimations. Under such framework, a new trajectory-segment is estimated by processing the N previous segments. Those correspond to a certain length of travelled path. The greater that length is, the more the measurements processed, thus anticipating a lower localization error, at the expense of course of a higher computational cost. The standard deviation of the phase noise is set to $\sigma_\phi = 0.1$ and the standard deviation of the encoders' noise is $\sigma_R = \sigma_L = 1cm$. Each trajectory segment is $0.1\,\mathrm{m}$ long. As a result, a previously travelled path of N segments corresponds to a length of $10Ncm$.

Fig. 24 demonstrates the achieved localization error at steady state with respect to the length of the processed trajectory and the multipath strength ρ. $0.2\,\mathrm{m}$ of previously travelled path ($N = 2$ segments) are not adequate and the localization error is higher than $0.15\,\mathrm{m}$ even for the convenient case of multipath absence, while an error of slightly lower than $0.4\,\mathrm{m}$ is reported in case of $\rho = 1$. The error decreases with the increase of the considered path's length, so is the impact of the multipath on the method's performance. When more than $1\,\mathrm{m}$ of traversed path ($N = 10$ previous segments) is exploited, the localization error drops to approximately zero, reporting a robustness for all tested multipath conditions.

Fig. 24 indicates that the effect of multipath on the method's performance depends on the length of the travelled path considered. In case of too short travelled paths ($0.2\,\mathrm{m}$ and $0.5\,\mathrm{m}$), the reported accuracy is different for each applied ratio ρ. For instance, when $0.2\,\mathrm{m}$ of previously travelled path is taken into account by the algorithm, a ratio value of $\rho = 1$ reports steady state error higher than $0.35\,\mathrm{m}$, while a value of $\rho = 0$ leads to an error of $0.15\,\mathrm{m}$. The influence of multipath decreases with the increase of the length of previously travelled path, since such increase corresponds to richer collections of data in a multipath-mitigation sense. Eventually, the method has equivalent performance under all tested multipath conditions when long enough paths ($2\,\mathrm{m}$ and $5\,\mathrm{m}$) are utilized.

Fig. 25 compares the execution-time required by the algorithm to process the data of N segments. In general, the algorithm's computational cost is dependent on the length of the previously traveled path considered, since longer paths correspond to more measurements processed. An estimation based on only $0.2\,\mathrm{m}$ of previous path requires on average slightly less than $0.03\,\mathrm{s}$. This value increases to $0.07\,\mathrm{s}$ when measurements collected within $5\,\mathrm{m}$ of previously travelled path are processed. Thanks to the deployment of non-linear optimization, the all reported valued of the time required for

Fig. 26: Photos of the environment the experiments were conducted in and the prototype RFID-equipped robot employed.

an estimation is orders of magnitude lower than a second.

V. Experimental Analysis

An experimental campaign was carried out in a laboratory room inside the campus, depicted in Fig. 26. The area is full of desks, chairs, electronic equipment, etc, thus forming a mulitpath-rich propagation environment full of scatterers. The prototype robot employed in the campaign is of unicycle differential-drive model [38] comprised by two independently controlled wheels. Both wheels are equipped with rotary encoders capable of measuring the incremental distances travelled by each of them. In addition to kinematic sensors, the robot carries a 2D LIght Detection And Ranging (LIDAR) sensor, thanks to which it is able to create the map of the environment and localize itself inside it through state-of-the-art algorithms. The LIDAR-based trajectories will be regarded as ground truth in the following analysis.

A commercial RFID reader is installed on board the vehicle, connected to two laterally positioned antennas, each of which is facing towards opposite direction. Consequently, as the robot is moving, they illuminate different half-spaces and interrogate different group of RFID tags each time. A total of 42 passive UHF RFID tags are placed at known locations inside the search space at a height of $0.8\,\mathrm{m}$ with an inter-tag distance of $0.5\,\mathrm{m}$.

The experiments took place in two stages. The first corresponds to the creation of the environment's map. The robot traverses inside the area and odometry and LIDAR readings are fused by a state-of-the-art algorithm [39]. Particularly, the mapping algorithm applies a Rao-Blackwellized particle filter, according to which each particle carries an individual map of the environment. Its key idea is to estimate the posterior distribution about potential maps and trajectories of the robot given its LIDAR observations and its odometry measurements. The mapping procedure is only performed once, at the first stage of experiments, and as soon as the map is completed, see Fig. 27, it is stored to be used in the second stage.

The second phase refers to the vehicle's tracking and the evaluation of the localization algorithms. The robot moves along different paths in a speed of approximately $8\,\mathrm{cm/s}$ and continuously collects and stores kinematic readings, LIDAR data and phase measurements from the surrounding RFID tags. Three different trajectories were tested as shown in Fig. 27: i) a simple straight path along the corridor formed by two rows of desks (20 employed tags), ii) an "aller-retour" path, i.e. the robot moves along a straight trajectory, performs a turn of 180° and goes on moving towards the opposite direction (20 tags) and iii) a Π-like trajectory (42 tags).

During this robot-localization stage, three different self-localization algorithms were deployed to estimate the robot's pose: i) an odometry-based algorithm that exploits only encoder readings, ii) a LIDAR-based algorithm that fuses encoder and LIDAR measurements and iii) the proposed RFID-based algorithm which combines odometry and RFID data.

In the case of the odometry-based trajectories, those are produced by exploiting equations (3) - (4) as described in section II-A. The initial location of the robot is considered known, since such algorithms are incapable of performing global localization. As far as the deployed LIDAR-based method [4] is concerned, the existence of a map is a prerequisite for robot localization. The algorithm rests on the alignment of LIDAR measurements to the map of the environment that is created in the mapping stage of the experiments. By employing Kalman of Particle filtering the algorithm also accounts for the robot's motion extracted by odometry observations. The LIDAR-based paths will be considered as the actual robot trajectories and the localization error of the odometry- and the RFID-based method will be computed with respect to them.

The RFID-based algorithm though, localizes the robot with respect to the coordinate system defined by the measured locations of the RFID tags. On the contrary, the LIDAR-based algorithm localizes the robot inside the previously generated map and thus, the produced poses refer to the coordinate system of the map with of course is different from the tag system. To compare the performance of the proposed RFID-based method with the LIDAR-based algorithm, all produced trajectories should refer to the same coordinate system. As a result, the tag locations have to be pinpointed inside the map and their coordinates to be transformed accordingly. It is anticipated that this manual procedure will introduce an error, which will contribute to the overall robot localization error.

The accuracy of the odometry-based trajectories depends among others on the length of the traversed path. The longer the robot has travelled, the more measurement error induced by the encoder-noise has been accumulated, leading to higher localization errors. An accurate commercial sensor typically requires trajectories of several meters to produce a significant deformation. In the conducted experiments, cable ducts were positioned at various locations on the floor of the room, in the expectation that faulty kinematic measurements will mislead the localization algorithms and cause deformations even from the first meters of robot's displacement. In fact, the ducts were placed such that only one of the two vehicle's wheels passes over them and erroneous measurements only from the one encoder will be gathered. Indeed, when the robot passes over such short obstacles, the disagreement in the measured distances of the two wheel produces a drift even though the robot moved along a straight line.

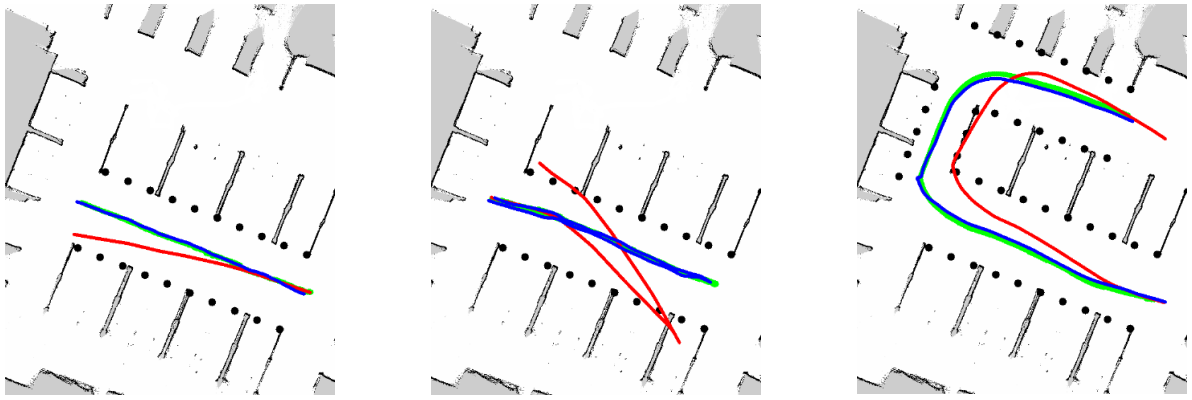

(a) straight trajectory (b) "aller-retour" trajectory (c) "Π"-shape trajectory

Fig. 27: Trajectories estimated by the proposed method combining odometry and RFID data (blue). They are compared to the trajectories estimated by exploiting odometry data only (red) and the trajectories estimated by processing odometry and LIDAR observations (green) regarded as the ground truth. Black circles represent tag locations. The trajectories are depicted inside the map of the environment. The initial location of the odometry-based trajectory is considered known, whilst the one of the RFID-based path not.

A. Experimental Results

Figs. 27 (a) - (c) contrast the trajectories estimated through different algorithms. The green path corresponds to the LIDAR-based path (regarded as ground truth), the red path is estimated by exploiting odometry data only, and the blue one refers to the proposed combination of odometry and RFID measurements. The initial location of the odometry-based trajectory is considered known, the same holds for the LIDAR-based trajectory (cannot perform global localization) whilst the initial location of the RFID-based path is unknown and the global localization problem is addressed. The pose of the robot is estimated every $2\,\mathrm{s}$ which corresponds to a spatial displacement of $0.15\,\mathrm{m}$. This value essentially represents the length of each trajectory-segment K. As shown, the cable ducts achieved to cause faulty drifts on the odometry-based paths producing results that have significant discrepancies with the actual trace. On the contrary, the RFID-based method is immune to such faulty measurements and the estimations almost coincide with the ground truth data.

Figs. 28 (a)-(f) illustrate the first steps of the proposed algorithm. Every new segment of trajectory estimated by the proposed method is represented by yellow color. Being SAR-based, the method depends on a rich collection of phase measurements to produce an accurate estimation. The first trajectory-segment is estimated on the basis of only a few data and therefore, the estimation is poor, Fig. 28 (a). The robot's estimated location may be in the vicinity of the actual one but it stills exhibits an important discrepancy.

The second trajectory segment is estimated on the basis of the first one. The estimated locations of the latter, accompanied by its phase observations, are inputted in system S_{ij}^{n}, participating in the calculation of the phase offset c_{ij}, which is common for both segments' measurements. Thanks to the estimation of this common term, the measurements of the two segments are associated with each other and since the difference between two consecutive phase measurements is small, so should be the corresponding difference between two consecutive antenna/robot locations as well. Therefore, to justify the small phase difference between the first measured sample of the second segment and the last phase sample of the first segment, the algorithm locates the beginning of the second segment at the end of the previous one, as indicated in Fig. 28 (b). Under such perspective, no jumps and discontinuities in the estimated trajectory are observed.

Aster the estimation of the second segment, the estimated trajectory so far is treated as a single segment and is re-estimated. Since a richer set of data is processed, the robot's location is corrected and the updated trajectory is moved closer to the actual one leading to a decrease in the localization error, Fig. 28 (c). The next segment is estimated based on the previous two (Fig. 28 (d)) and the whole trajectory consisted of all three segments is re-estimated again, Fig. 28 (e). Now the actual and the estimated locations almost coincide. The described procedure continuous as long as the vehicle is moving.

Figs. 29 - 31 quantify the dissimilarities of the trajectories of Fig. 27 presenting the localization error with respect to the covered distance of the robot. The trajectory estimated by exploiting odometry data only, increases with the travelled distance as expected. The error induced by the sensor noise piles up as the robot covers longer distances, eventually leading to significantly high localization errors. On the contrary, when odometry data are combined with RFID measurements, the achieved accuracy is independent of the traversed path. In section IV the numerical analysis demonstrated the ineffectiveness of the method when a single antenna is employed. This arose the need of mounting reference tags at both sides of the robot's trace and installing two antennas on board the robotic vehicle that are facing towards opposite directions. This is verified through the experimental investigation, too, since the performance of the method strongly depends on the antenna population. When a single antenna is used, the performance

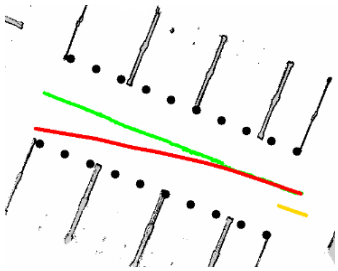

(a) Estimation of the 1^{st} trajectory-segment (yellow). The estimated segment is in the vicinity of the actual (green), but not satisfactorily close.

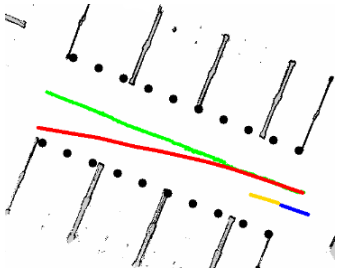

(b) Estimation of the 2^{nd} trajectory-segment (yellow). The estimation is based on the previously travelled path (blue).

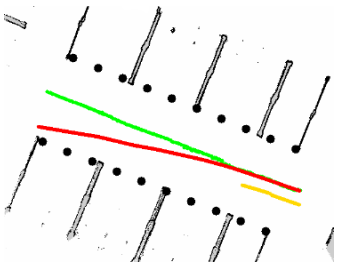

(c) Correction of the whole estimated trajectory (yellow). The distance between the estimated trajectory and the actual (green) has been decreased.

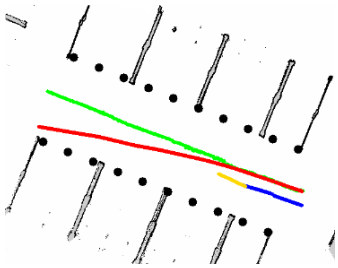

(d) Estimation of the 3^{rd} trajectory-segment (yellow). The estimation is based on the previously travelled path (blue).

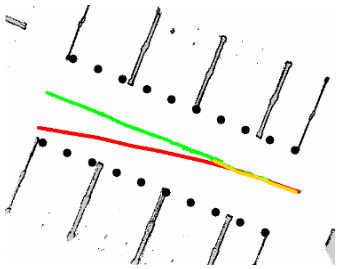

(e) Correction of the whole estimated trajectory (yellow). The estimated trajectory now coincides with the actual (green).

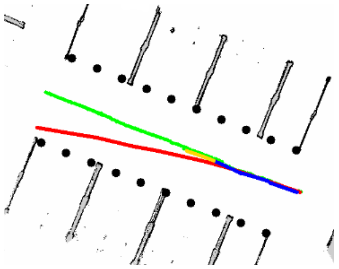

(f) Estimation of the 4^{th} trajectory-segment (yellow). The estimation is based on the previously travelled path (blue).

Fig. 28: The progress of the global localization of the robot over time from the initial up to the fourth trajectory-segment. The trajectory estimated by exploiting odometry data only is depicted by red, the trajectory estimated by exploiting odometry and LIDAR data is depicted by green and the trajectory estimated by exploiting odomerty and RFID data (proposed method) is depicted by blue; the current segment is depicted by yellow. Black circles represent tag locations. The trajectories are depicted inside the map of the environment. The initial location of the odometry-based trajectory (red) and LIDAR-based (green) is considered known, whilst the one of the RFID-based (blue) path not.

of the method is not robust and the produced error fluctuates. Instead, the deployment of two antennas deliver significantly better results reporting localization errors that never exceed the $0.2\,\mathrm{m}$.

Table 1 summarizes the average error achieved by each algorithm for all experiments. When only odometry data are exploited, the mean localization error is $0.45\,\mathrm{m}$, even though the initial pose of the robot were known. This value approximately drops to half $(0.25\,\mathrm{m})$ when a RFID-based algorithm is employed utilizing a single antenna, while best accuracy is delivered when RFID data by two antennas are combined, reporting a mean error of slightly less than $0.1\,\mathrm{m}$.

	odometry-based		**RFID-based (1 antenna)**		**RFID-based (2 antennas)**	
route	**mean**	**std**	**mean**	**std**	**mean**	**std**
straight	0.24	0.19	0.16	0.06	0.08	0.07
"aller-retour"	0.57	0.37	0.23	0.09	0.09	0.04
"Π"-shape	0.43	0.19	0.29	0.09	0.1	0.03
total	0.44	0.26	0.24	0.08	0.09	0.04

TABLE I: Average achieved localization error of the odometry-based algorithm against the RFID-based method when the latter employs a single or two antennas. All values are expressed in meters.

B. Performance vs Length of previously Travelled Path considered

This analysis explores the method's effectiveness with respect to the length of the previously travelled trajectory taken into account for the estimation of a new trajectory segment. As already described, the greater that length is, the wealthier the collection of processed measurements, thus leading to a lower localization error, at the expense of a higher computational cost.

Fig. 32 presents the mean localization error of all experiments for the case of two utilized antennas. When no previous data are taken into account the error is quite high in the order of $0.5\,\mathrm{m}$. Same accuracy is achieved for the insufficient length of only $0.15\,\mathrm{m}$. However, the effectiveness is improved with the increase of the length achieving a mean error of around $0.1\,\mathrm{m}$ for paths longer than $0.5\,\mathrm{m}$. The method reports equivalent accuracy for longer considered trajectories and the error is maintained at same levels.

The algorithm estimates the robot's pose by solving a data-fit problem through non-linear optimization. The greatest

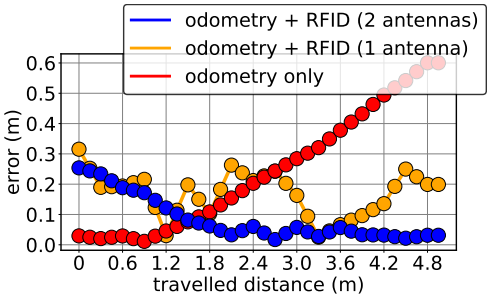

Fig. 29: Measured localization error with respect to its travelled path for the trajectory of Fig. 27 (a).

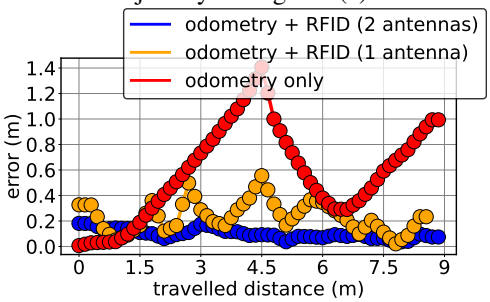

Fig. 30: Measured localization error with respect to its travelled path for the trajectory of Fig. 27 (b).

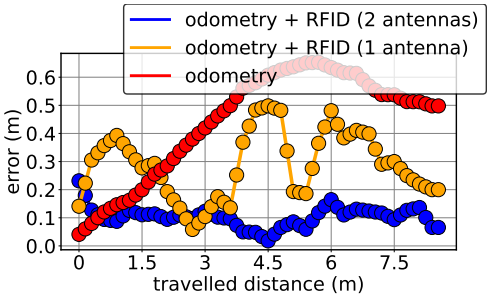

Fig. 31: Measured localization error with respect to its travelled path for the trajectory of Fig. 27 (c).

advantage of the proposed method is its ability to rapidly converge to the minimum of the problem which corresponds to the robot's optimum pose. As a result, the computational cost and the execution time required for a single estimation is insignificant. This effect is depicted in Fig. 33, which compares the run-time required for the algorithm to perform a single estimation of the robot's pose with respect to the length of the previously travelled path considered. The execution time is realised as the time required for phase unwrapping and the time required to solve the data-fit problem. As the length of previously travelled path considered increases, the mean time to localize the robot is increased, since the processing of the more data collected upon a longer path demands for higher run-time. However, all reported execution times are lower than $0.5\,\mathrm{s}$ even for the case of a $3\,\mathrm{m}$-long path. Since the vehicle's pose is updated every $2\,\mathrm{s}$ and the average time required for pose-estimation is significantly lower than this value, the real-time capability of the method is verified. Thanks to its low execution time, the proposed scheme can even afford a decrease in the estimation-step by a factor of 4, i.e. the robot's pose can be updated every half a second.

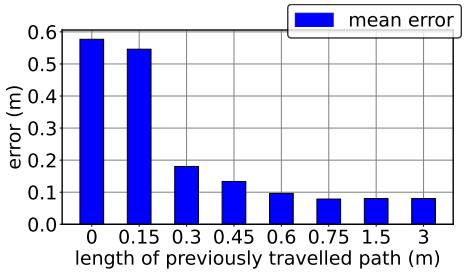

Fig. 32: Mean localization error with respect to the length of the previously travelled path that is taken into account by the estimation algorithm. Two antennas are employed.

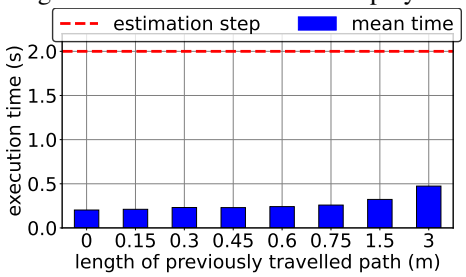

Fig. 33: Mean execution time required for the estimation of the robot's pose with respect to the length of the previously travelled path that is taken into account by the estimation algorithm. Two antennas are employed.

VI. Conclusion

This work deals with the problem of recovering a mobile robot's location and direction in the global frame of reference without knowledge of the robot's starting state, exploiting RFID technology. The robot is realised as a differential-drive vehicle and is equipped with kinematic sensors on its wheels to measure the incremental distances covered by each of them and includes an RFID reader to collect phase measurements from reference tags positioned at known locations throughout the environment.

Tracking of the mobile robot over time is accomplished by processing short segments of trajectory each time. Odometry data collected by the wheel sensors produce a trajectory segment relative to an unknown initial position. Odometry is not expected to suffer from large errors during small travelled segments. The algorithm attempts to rotate and move each new segment throughout the map, in order to better fit its actual position based on phase-measurements collected by RFID tags. In that manner, it does not allow odometry errors to pile up. The odometry-based relative trajectory of the robot-mounted antennas, the known positions of the surrounding RFID tags, the unwrapped phase measurements collected by them, and a phase-to-distance theoretical model are inputted to a data-fit problem. The latter is rapidly solved by state-of-the-art nonlinear optimization techniques and the unknown initial pose of trajectory-segment in the absolute frame is recovered.

A numerical analysis investigates the impact of different features of the algorithm on the method's effectiveness. It also demonstrates that the installation of two antennas facing opposite directions on board the vehicle is a basic requirement for the method's operability. A prototype robot was employed

to carry out an experimental campaign and the RFID-based localization method was compared against an odometry- and LIDAR-based method. Experimental results report a mean localization error smaller than $0.1\,\mathrm{m}$ while the real-time capability of the method is verified.

REFERENCES

[1] Jin-Xia Yu, Zi-Xing Cai and Zhuo-Hua Duan, "Dead reckoning of mobile robot in complex terrain based on proprioceptive sensors," 2008 International Conference on Machine Learning and Cybernetics, Kunming, China, 2008, pp. 1930-1935, doi: 10.1109/ICMLC.2008.4620722.

[2] K. Chen, B. T. Lopez, A. -a. Agha-mohammadi and A. Mehta, "Direct LIDAR Odometry: Fast Localization With Dense Point Clouds," in IEEE Robotics and Automation Letters, vol. 7, no. 2, pp. 2000-2007, April 2022, doi: 10.1109/LRA.2022.3142739.

[3] D. Alejo, F. Caballero and L. Merino, "RGBD-based robot localization in sewer networks," 2017 IEEE/RSJ International Conference on Intelligent Robots and Systems (IROS), Vancouver, BC, Canada, 2017, pp. 4070-4076, doi: 10.1109/IROS.2017.8206263.

[4] Filotheou, A., Tsardoulias, E., Dimitriou, A. et al. Pose Selection and Feedback Methods in Tandem Combinations of Particle Filters with Scan-Matching for 2D Mobile Robot Localisation. J Intell Robot Syst 100, 925–944 (2020). https://doi.org/10.1007/s10846-020-01253-6

[5] Filotheou, A., Tzitzis, A., Tsardoulias, E. et al. Passive Global Localisation of Mobile Robot via 2D Fourier-Mellin Invariant Matching. J Intell Robot Syst 104, 26 (2022), https://doi.org/10.1007/s10846-021-01535-7

[6] X. Deng, A. Mousavian, Y. Xiang, F. Xia, T. Bretl and D. Fox, "PoseRBPF: A Rao–Blackwellized Particle Filter for 6-D Object Pose Tracking," in IEEE Transactions on Robotics, vol. 37, no. 5, pp. 1328-1342, Oct. 2021, doi: 10.1109/TRO.2021.3056043.

[7] A. Filotheou, G. D. Sergiadis and A. G. Dimitriou, "FSM: Correspondenceless scan-matching of panoramic 2D range scans," 2022 IEEE/RSJ International Conference on Intelligent Robots and Systems (IROS), Kyoto, Japan, 2022, pp. 6968-6975, doi: 10.1109/IROS47612.2022.9981228.

[8] G. Wang, X. Wu, S. Jiang, Z. Liu and H. Wang, "Efficient 3D Deep LIDAR Odometry," in IEEE Transactions on Pattern Analysis and Machine Intelligence, 2022, doi: 10.1109/TPAMI.2022.3207015.

[9] N. Engel, S. Hoermann, M. Horn, V. Belagiannis and K. Dietmayer, "DeepLocalization: Landmark-based Self-Localization with Deep Neural Networks," 2019 IEEE Intelligent Transportation Systems Conference (ITSC), Auckland, New Zealand, 2019, pp. 926-933, doi: 10.1109/ITSC.2019.8917005.

[10] W. Chen, J. Xu, X. Zhao, Y. Liu and J. Yang, "Separated Sonar Localization System for Indoor Robot Navigation," in IEEE Transactions on Industrial Electronics, vol. 68, no. 7, pp. 6042-6052, July 2021, doi: 10.1109/TIE.2020.2994856.

[11] Aulinas, Josep, et al. "The SLAM problem: a survey." Artificial Intelligence Research and Development (2008): 363-371.

[12] A. Motroni, A. Buffi and P. Nepa, "A Survey on Indoor Vehicle Localization Through RFID Technology," in IEEE Access, vol. 9, pp. 17921-17942, 2021, doi: 10.1109/ACCESS.2021.3052316.

[13] E. DiGiampaolo and F. Martinelli, "A Passive UHF-RFID System for the Localization of an Indoor Autonomous Vehicle," in IEEE Transactions on Industrial Electronics, vol. 59, no. 10, pp. 3961-3970, Oct. 2012, doi: 10.1109/TIE.2011.2173091.

[14] L. Yang, J. Cao, W. Zhu and S. Tang, "Accurate and Efficient Object Tracking Based on Passive RFID," in IEEE Transactions on Mobile Computing, vol. 14, no. 11, pp. 2188-2200, 1 Nov. 2015, doi: 10.1109/TMC.2014.2381232.

[15] A. Codas, M. Devy and C. Lemaire, "Robot localization algorithm using odometry and RFID technology", IFAC Proc. Volumes, vol. 43, no. 16, pp. 569-574, 2010.

[16] P. Vorst and A. Zell, "Fully autonomous trajectory estimation with long-range passive RFID," 2010 IEEE International Conference on Robotics and Automation, Anchorage, AK, USA, 2010, pp. 1867-1872, doi: 10.1109/ROBOT.2010.5509810.

[17] Gameiro, Duarte Lopes. "Indoors Localization of a Robot Using RFID Tags." (2015).

[18] S. S. Saab and Z. S. Nakad, "A Standalone RFID Indoor Positioning System Using Passive Tags," in IEEE Transactions on Industrial Electronics, vol. 58, no. 5, pp. 1961-1970, May 2011, doi: 10.1109/TIE.2010.2055774.

[19] S. Park and H. Lee, "Self-Recognition of Vehicle Position Using UHF Passive RFID Tags," in IEEE Transactions on Industrial Electronics, vol. 60, no. 1, pp. 226-234, Jan. 2013, doi: 10.1109/TIE.2012.2185018.

[20] C. -H. Huang, L. -H. Lee, C. C. Ho, L. -L. Wu and Z. -H. Lai, "Real-Time RFID Indoor Positioning System Based on Kalman-Filter Drift Removal and Heron-Bilateration Location Estimation," in IEEE Transactions on Instrumentation and Measurement, vol. 64, no. 3, pp. 728-739, March 2015, doi: 10.1109/TIM.2014.2347691.

[21] J. J. Pomárico-Franquiz and Y. S. Shmaliy, "Accurate Self-Localization in RFID Tag Information Grids Using FIR Filtering," in IEEE Transactions on Industrial Informatics, vol. 10, no. 2, pp. 1317-1326, May 2014, doi: 10.1109/TII.2014.2310952.

[22] E. DiGiampaolo and F. Martinelli, "Mobile Robot Localization Using the Phase of Passive UHF RFID Signals," in IEEE Transactions on Industrial Electronics, vol. 61, no. 1, pp. 365-376, Jan. 2014, doi: 10.1109/TIE.2013.2248333.

[23] F. Martinelli, "A Robot Localization System Combining RSSI and Phase Shift in UHF-RFID Signals," in IEEE Transactions on Control Systems Technology, vol. 23, no. 5, pp. 1782-1796, Sept. 2015, doi: 10.1109/TCST.2014.2386777.

[24] B. Tao, H. Wu, Z. Gong, Z. Yin and H. Ding, "An RFID-Based Mobile Robot Localization Method Combining Phase Difference and Readability," in IEEE Transactions on Automation Science and Engineering, vol. 18, no. 3, pp. 1406-1416, July 2021, doi: 10.1109/TASE.2020.3006724.

[25] E. DiGiampaolo, F. Martinelli and F. Romanelli, "A Localization System for Autonomous Vehicles Based on TriLateration Tags," 2022 16th European Conference on Antennas and Propagation (EuCAP), Madrid, Spain, 2022, pp. 1-5, doi: 10.23919/EuCAP53622.2022.9768963.

[26] V. Magnago et al., "Ranging-Free UHF-RFID Robot Positioning Through Phase Measurements of Passive Tags," in IEEE Transactions on Instrumentation and Measurement, vol. 69, no. 5, pp. 2408-2418, May 2020, doi: 10.1109/TIM.2019.2960900.

[27] A. Motroni, A. Buffi, P. Nepa and B. Tellini, "Sensor-Fusion and Tracking Method for Indoor Vehicles With Low-Density UHF-RFID Tags," in IEEE Transactions on Instrumentation and Measurement, vol. 70, pp. 1-14, 2021, Art no. 8001314, doi: 10.1109/TIM.2020.3027926.

[28] A. Parr, R. Miesen and M. Vossiek, "Inverse SAR approach for localization of moving RFID tags," 2013 IEEE International Conference on RFID (RFID), Orlando, FL, USA, 2013, pp. 104-109, doi: 10.1109/RFID.2013.6548142.

[29] J. H. Teo, A. Loganathan, P. Goh, and N. S. Ahmad, "Autonomous mobile robot navigation via RFID signal strength sensing," Int. J. Mech. Eng. Robot. Res., vol. 9, no. 8, pp. 1140-1144, 2020.

[30] R. Liu, G. Huskić and A. Zell, "Dynamic objects tracking with a mobile robot using passive UHF RFID tags," 2014 IEEE/RSJ International Conference on Intelligent Robots and Systems, Chicago, IL, USA, 2014, pp. 4247-4252, doi: 10.1109/IROS.2014.6943161.

[31] W. Gueaieb and M. S. Miah, "Mobile robot navigation using particle swarm optimization and noisy RFID communication," 2008 IEEE International Conference on Computational Intelligence for Measurement Systems and Applications, Istanbul, Turkey, 2008, pp. 111-116, doi: 10.1109/CIMSA.2008.4595843.

[32] Martinelli, F. Simultaneous Localization and Mapping Using the Phase of Passive UHF-RFID Signals. J Intell Robot Syst 94, 711–725 (2019). https://doi.org/10.1007/s10846-018-0903-8

[33] F. Romanelli, F. Martinelli and E. D. Giampaolo, "Robust Simultaneous Localization and Mapping Using Range and Bearing Estimation of Radio Ultra High Frequency Identification Tags," in IEEE Transactions on Control Systems Technology, vol. 31, no. 2, pp. 772-785, March 2023, doi: 10.1109/TCST.2022.3204386.

[34] G. Mylonopoulos, A. R. Chatzistefanou, A. Filotheou, A. Tzitzis, S. Siachalou and A. G. Dimitriou, "Localization, Tracking and Following a Moving Target by an RFID Equipped Robot," 2021 IEEE International Conference on RFID Technology and Applications (RFID-TA), Delhi, India, 2021, pp. 32-35, doi: 10.1109/RFID-TA53372.2021.9617436.

[35] A. Tzitzis et al., "Localization of RFID Tags by a Moving Robot, via Phase Unwrapping and Non-Linear Optimization," in IEEE Journal of Radio Frequency Identification, vol. 3, no. 4, pp. 216-226, Dec. 2019, doi: 10.1109/JRFID.2019.2936969.

[36] A. Tzitzis et al., "Trajectory Planning of a Moving Robot Empowers 3D Localization of RFID Tags with a Single Antenna," in IEEE Journal of Radio Frequency Identification, doi: 10.1109/JRFID.2020.3000332.

[37] A. Tzitzis, A. Raptopoulos Chatzistefanou, T. V. Yioultsis and A. G. Dimitriou, "A Real-Time Multi-Antenna SAR-Based Method for 3D Localization of RFID Tags by a Moving Robot," in IEEE Journal of Radio Frequency Identification, vol. 5, no. 2, pp. 207-221, June 2021, doi: 10.1109/JRFID.2021.3070409.

[38] F. Kappeler, "Unicycle Robot", 2007. Accessed: 3 May 2023 [Online]. Available: https://www.epfl.ch/labs/la/wp-content/uploads/2018/08/Kappeler.Rapport.pdf.pdf

[39] G. Grisetti, C. Stachniss and W. Burgard, "Improved Techniques for Grid Mapping With Rao-Blackwellized Particle Filters," in IEEE Transactions on Robotics, vol. 23, no. 1, pp. 34-46, Feb. 2007, doi: 10.1109/TRO.2006.889486.

[40] M. A. Branch, T. F. Coleman, and Y. Li, "A Subspace, Interior, and Conjugate Gradient Method for Large-Scale Bound-Constrained Minimization Problems," *SIAM Journal on Scientific Computing*, vol. 21, no. 1, pp. 1–23, 1999.

[41] R. H. Byrd, R. B. Schnabel, and G. A. Shultz, "Approximate Solution of the Trust Region Problem by Minimization over Two-Dimensional Subspaces," *Mathematical Programming*, vol. 40, pp. 247–263, 1988.

[42] J. J. More and D. C. Sorensen, "Computing a Trust Region Step," *SIAM Journal on Scientific and Statistical Computing*, vol. 3, pp. 553–572, 1983.

[43] A. G. Dimitriou, S. Siachalou, A. Bletsas and J. N. Sahalos, "A Site-Specific Stochastic Propagation Model for Passive UHF RFID," in IEEE Antennas and Wireless Propagation Letters, vol. 13, pp. 623-626, 2014, doi: 10.1109/LAWP.2014.2313350.